

Revisiting $B_s \rightarrow PP$ and PV Decays with Contributions from ϕ_{B2} with perturbative QCD approach

Yueling Yang¹, Zhao-Jie Lü¹, Su-Ping Jin¹*, and Junfeng Sun¹

¹Institute of Particle and Nuclear Physics, Henan Normal University, Xinxiang 453007, China

February 25, 2025

Abstract

The $B_s \rightarrow PP$ and PV decay modes are revisited at leading order within the perturbative QCD approach, incorporating the B_s mesonic wave function (WF) ϕ_{B2} . Here, P represents the pseudoscalar mesons π and K , while V denotes the ground-state vector mesons. The investigation incorporates two key refinements: the contribution of the sub-leading twist WF ϕ_{B2} of the B_s meson and the effects of higher-order terms in the distribution amplitudes (DAs) of the final-state mesons. Employing the minimum χ^2 method, we optimize the shape parameter ω_{B_s} of the B_s meson WF and systematically calculate the branching ratios and CP violation parameters for these decay modes. Our results demonstrate that the inclusion of ϕ_{B2} significantly impacts both the branching ratios and CP asymmetries, offer an improved agreement with existing experimental data for specific channels. This underscores the necessity of accounting for ϕ_{B2} in theoretical studies of B_s weak decays. While the higher-order corrections in the final-state meson DAs yield comparatively smaller effects, they still enhance the theoretical predictions. These findings highlight the importance of refining both wave function modeling and higher-order contributions in pQCD calculations. Future high-precision experimental measurements will further test these predictions, while continued theoretical efforts are essential to explore additional interaction mechanisms and systematic uncertainties. The interplay between experimental advancements and theoretical improvements remains critical for a deeper understanding of B_s meson decay dynamics.

*E-mail: jinsuping@htu.edu.cn (corresponding author)

1 Introduction

B meson physics represents a vital frontier in particle physics, driven by continuous advancements in both experimental techniques and theoretical understanding. The field is entering an era of unprecedented data collection through major experimental initiatives: the Belle-II experiment at the SuperKEKB e^+e^- collider is progressing toward its design goal of 50 ab^{-1} integrated luminosity [1], while the upgraded LHCb detector at the High Luminosity LHC(HL-LHC) anticipates collecting approximately 300 fb^{-1} [2]. These efforts will be complemented by next-generation e^+e^- collider projects – notably the Circular Electron-Positron Collider (CEPC) [3] and FCC-ee [4] – which are projected to generate over 10^{10} B_s mesons via Z^0 boson decays. This impressive yield arises from two key factors: the substantial $Z^0 \rightarrow b\bar{b}$ branching fraction of $\mathcal{B}(Z^0 \rightarrow b\bar{b}) \approx 15.12\%$ [5], combined with the b-quark fragmentation fraction to B_s mesons of $f(b \rightarrow B_s) \approx 10.3\%$ [6, 7]. The relatively low fragmentation fraction compared to $B_{u,d}$ mesons ($\sim 40\%$) reflects the suppressed production mechanism for B_s during hadronization [7], making high-statistics studies particularly valuable for probing rare processes.

The particular importance of $B_s \rightarrow PP$ and PV decays (where P denotes light pseudoscalar mesons and V represents light vector mesons) lies in their unique potential to probe both Standard Model predictions and potential New Physics scenarios. These processes serve as sensitive testing grounds for understanding QCD dynamics in heavy quark decays, investigating CP violation mechanisms, and constraining the unitarity triangle parameters. Moreover, they offer complementary information to their B_d and B_u counterparts due to the distinct penguin contributions and oscillation characteristics of the B_s system. The interplay between theoretical calculations and experimental results in this sector continues to be crucial for verifying the consistency of the SM and identifying possible anomalies that might indicate physics beyond current paradigms.

Over the past years, significant progress has been made in understanding two-body charmless hadronic decays $B_s \rightarrow PP$ and PV , with extensive experimental measurements and theoretical investigations. Among the possible $B_s \rightarrow PP$ and PV decay channels, experimental collaborations including CDF [8–11], Belle [12, 13], and LHCb [14–21] have successfully observed seven channels to date. The current experimental status, including measurements of branching ratios and CP -violating asymmetries for these decays, has been systematically compiled in Table 1. With the anticipated high-precision data from upgraded facilities like LHCb and Belle-II [5, 22], significant improvements in both statistical significance and systematic uncertainties are expected in forthcoming measurements. From the theoretical perspective, $B_s \rightarrow PP$ and PV decays have been extensively investigated through various approaches, including QCD factorization [23–26], soft-collinear effective theory (SCET) [27], and perturbative QCD (pQCD) factorization approach [28–33], as well as flavor SU(3) symmetry

Table 1: The measured values of the branching ratios (in units of 10^{-6}) of the seven considered decay modes and $A_{\text{CP}}(B_s^0 \rightarrow \pi^+ K^-)$ of $B_s^0 \rightarrow K^+ K^-$ decay, as reported by the Belle[12, 13], CDF[8–11], LHCb Collaboration [14–21], and the world averages as given in Refs. [5, 22].

Mode	Belle[12, 13]	CDF[8–11]	LHCb[14–21]	PDG[5]	HFLAV[22]
$\mathcal{B}(\bar{B}_s^0 \rightarrow \pi^- K^+)$	< 26	5.8 ± 1.12	$6.0 \pm 0.7 \pm 0.6$	5.9 ± 0.7	$6.1^{+0.9}_{-0.8}$
$\mathcal{B}(\bar{B}_s^0 \rightarrow \pi^+ \pi^-)$	< 12	0.65 ± 0.19	$0.75 \pm 0.09 \pm 0.07$	0.72 ± 0.1	$0.74^{+0.12}_{-0.10}$
$\mathcal{B}(\bar{B}_s^0 \rightarrow K^+ K^-)$	$38^{+10}_{-9} \pm 7$	28.3 ± 3.6	$25.7 \pm 1.7 \pm 2.5$	27.2 ± 2.3	$27.4^{+3.2}_{-2.8}$
$\mathcal{B}(\bar{B}_s^0 \rightarrow K^0 \bar{K}^0)$	$19.6^{+5.8}_{-5.1} \pm 2.0$	—	$1.68 \pm 3.4^{+1.6}_{-1.5}$	17.6 ± 3.1	17.4 ± 3.1
$\mathcal{B}(\bar{B}_s^0 \rightarrow K^\pm \bar{K}^{*\mp})$	—	—	$18.6 \pm 1.2 \pm 4.5$	19.0 ± 5	18.6 ± 4.7
$\mathcal{B}(\bar{B}_s^0 \rightarrow \bar{K}^{*0} K^0)$	—	—	$19.8 \pm 2.8 \pm 5$	20.0 ± 6.0	19.8 ± 5.7
$\mathcal{B}(\bar{B}_s^0 \rightarrow \pi^- K^{*+})$	—	—	$2.9 \pm 1.0 \pm 0.2$	2.9 ± 1.1	3.0 ± 1.1
$A_{\text{CP}}(B_s^0 \rightarrow K^- \pi^+)$	0.22 ± 0.07	—	0.236 ± 0.017	0.224 ± 0.012	—
		—	0.213 ± 0.017		

analyses [34, 35]. While these methods exhibit substantial differences in their predictions for CP-violating asymmetry patterns and magnitudes, they demonstrate reasonable consistency in branching ratio predictions when considering current theoretical uncertainties.

In our previous investigation [36, 37], we conducted a systematic reanalysis of $B \rightarrow PP$ and PV decays within the pQCD framework. These studies incorporated two crucial enhancements: the inclusion of subleading-twist wave functions (WFs) for the B meson and updated distribution amplitudes (DAs) for final-state pseudoscalar mesons. Notably, our findings revealed that the B -mesonic WF component ϕ_{B2} - frequently overlooked in prior studies - exerts distinct influence on both hadronic matrix elements (HMEs) and branching ratios, with magnitude comparable to next-to-leading-order (NLO) corrections.

Building upon these insights, the present work extends this analysis to charmless $B_s \rightarrow PP$ and PV decay channels. This extension aligns with recent advancements in both theoretical precision and experimental resolution. Our current investigation maintains focus on $P = \{\pi, K\}$ final states, deliberately excluding η and η' mesons due to persistent theoretical challenges in resolving their flavor mixing structure and potential glueball admixtures. By incorporating this subleading-twist WFs for the B_s meson, we systematically enhance the theoretical framework, leading to the following findings:

- We demonstrate that the ϕ_{B2} term contributes zero in factorizable annihilation topologies. This property provides a crucial basis for simplifying theoretical calculations of the corresponding

decay channels.

- By fully incorporating the ϕ_{B_2} term, we observe substantial corrections to the branching ratios of various decay channels, ranging from 1.4% to 59.4%. Notably, in the decay channel $\bar{B}_s^0 \rightarrow K^- K^+$, this correction reduces the discrepancy between theoretical predictions and the latest LHCb experimental data from 43% to 17%, thereby validating the necessity of higher-order wave function terms for enhancing theoretical precision. In certain decay channels, such as $\bar{B}_s^0 \rightarrow \pi^0 K^0$, $\bar{B}_s^0 \rightarrow K^- K^+$, and $\bar{B}_s^0 \rightarrow \bar{K}^0 K^0$, the contribution of the ϕ_{B_2} term is comparable to that of next-to-leading order corrections.
- Numerical results indicate that variations in the Gegenbauer moments $a_2^{P(V)}$ within the specified input parameter ranges lead to average fluctuations of approximately 7% to 10% in the branching ratios. This underscores the importance of accurately optimizing non-perturbative parameters.
- After including traditionally neglected higher-order terms in the DAs of final-state mesons, we find that the changes in branching ratios are less than 6%. This result demonstrates the stability of the existing theoretical framework concerning higher-order terms and supports the validity of certain approximations within the pQCD approach.

The structure of this paper is organized as follows. In Section 2, we briefly outline the theoretical framework underlying the analysis including effective Hamiltonian and decay amplitudes. Section 3 defines the relevant kinematic and provides the expressions for WFs involved in the decays. We reevaluate the branching ratios and CP asymmetries for the $B_s \rightarrow PP$ and PV decays, considering the effects of the B_s -mesonic wave function ϕ_{B_2} and present the numerical results in Section 4. The paper concludes with a summary in Section 5. Additional details on the building blocks and the decay amplitudes for the $B_s \rightarrow PP$ and PV decays can be found in Appendix A.

2 EFFECTIVE HAMILTONIAN AND DECAY AMPLITUDES

At the quark level, The low-energy effective Hamiltonian for the decays $\bar{B}_s^0 \rightarrow PP$ and PV can be expressed as the product of Wilson coefficients and effective operators,

$$\mathcal{H}_{\text{eff}} = \frac{G_F}{\sqrt{2}} \sum_{q=d,s} \left\{ V_{ub} V_{uq}^* \sum_{i=1}^2 C_i(\mu) \mathcal{O}_i - V_{tb} V_{tq}^* \sum_{j=3}^{10} C_j(\mu) \mathcal{O}_j \right\} + h.c., \quad (1)$$

where G_F is the Fermi coupling constant, V_i are the elements of the Cabibbo-Kobayashi-Maskawa (CKM) matrix, $C_i(\mu)$ are the Wilson coefficients evaluated at the energy scale μ , and \mathcal{O}_i are the effective operators corresponding to specific decay processes.

Utilizing the phenomenological Wolfenstein parametrization up to $\mathcal{O}(\lambda^8)$, the CKM factors read

$$V_{ub} V_{us}^* = A \lambda^4 (\rho - i \eta) + \mathcal{O}(\lambda^8), \quad (2)$$

$$V_{ub} V_{ud}^* = A \lambda^3 (\rho - i \eta) \left(1 - \frac{1}{2} \lambda^2 - \frac{1}{8} \lambda^4\right) + \mathcal{O}(\lambda^8), \quad (3)$$

$$V_{tb} V_{td}^* = A \lambda^3 + A^3 \lambda^7 \left(\rho - i \eta - \frac{1}{2}\right) - V_{ub} V_{ud}^* + \mathcal{O}(\lambda^8), \quad (4)$$

$$V_{tb} V_{ts}^* = -A \lambda^2 \left(1 - \frac{1}{2} \lambda^2 - \frac{1}{8} \lambda^4\right) + \frac{1}{2} A^3 \lambda^6 - V_{ub} V_{us}^* + \mathcal{O}(\lambda^8). \quad (5)$$

The parameters A , λ , ρ , and η correspond to the Wolfenstein parametrization of the CKM matrix. The most recent fitted values for these parameters can be found in Ref.[5]. A summary of these fitted values is provided in Table 2.

In the SM, the decay amplitude for $\bar{B}_s^0 \rightarrow PM$ ($M = P, V$) can be expressed as:

$$\mathcal{A}(\bar{B}_s^0 \rightarrow PM) = \langle PM | \mathcal{H}_{\text{eff}} | \bar{B}_s^0 \rangle = \frac{G_F}{\sqrt{2}} \sum_{i=1}^{10} V_i C_i \langle PM | \mathcal{O}_i | \bar{B}_s^0 \rangle. \quad (6)$$

The HMEs $\langle \mathcal{O}_i \rangle \equiv \langle PM | \mathcal{O}_i | \bar{B}_s^0 \rangle$ describe the transition from quarks to hadrons. These matrix elements involve energy scales that lie between the perturbative and non-perturbative regimes. In the pQCD approach, by retaining the transverse momentum of the quarks and introducing Sudakov factors, the HMEs can be written in a convolution form, incorporating both the perturbative (hard scattering kernel) and non-perturbative (universal hadronic WF) parts. Thus, the decay amplitude can be factorized into the convolution of three parts: the Wilson coefficients C_i , the hard scattering kernel \mathcal{H}_i , and the hadronic WFs. Therefore, the HMEs for the $\bar{B}_s^0 \rightarrow PM$ decay process can be written as

$$\begin{aligned} \langle PM | C_i \mathcal{O}_i | \bar{B}_s^0 \rangle &\propto \int dx_1 dx_2 dx_3 db_1 db_2 db_3 C_i(t_i) \mathcal{H}_i(x_1, x_2, x_3, b_1, b_2, b_3) \\ &\times \Phi_{B_s}(x_1, b_1) e^{-S_{B_s}} \Phi_P(x_2, b_2) e^{-S_P} \Phi_M(x_3, b_3) e^{-S_M}, \end{aligned} \quad (7)$$

where b_i denotes the conjugate variable of the transverse momentum $\vec{k}_{i\perp}$ of the valence quarks; \mathcal{H}_i represents the scattering amplitudes for hard gluon exchange interactions among the quarks; and e^{-S_i} is the Sudakov factor. Additional variables and input parameters are described in the following section.

3 KINEMATICS AND THE WAVE FUNCTIONS

The momenta of the \bar{B}_s^0 meson p_B , recoiling meson M_2 (p_2), and emitted meson M_3 (p_3), along with their corresponding parton momenta, are defined in light-cone coordinates as

$$\begin{aligned} p_B &= \frac{m_B}{\sqrt{2}}(1, 1, 0), & k_1 &= (x_1 \frac{m_B}{\sqrt{2}}, 0, \vec{k}_{1\perp}), \\ p_2 &= \frac{m_B}{\sqrt{2}}(0, 1, 0), & k_2 &= (0, x_2 \frac{m_B}{\sqrt{2}}, \vec{k}_{2\perp}), \\ p_3 &= \frac{m_B}{\sqrt{2}}(1, 0, 0), & k_3 &= (x_3 \frac{m_B}{\sqrt{2}}, 0, \vec{k}_{3\perp}), \end{aligned} \quad (8)$$

which are shown in Fig. 1. Here m_{B_s} denotes the B_s meson mass, while x_i represent the longitudinal momentum fractions carried by the constituent partons. The transverse momentum components $\vec{k}_{i\perp}$ in Eq. (9) are treated as suppressed degrees of freedom. For the vector meson, we also take into account its longitudinal polarization vector, given by $e_V^\parallel = \frac{p_V}{m_V} - \frac{m_V}{p_V \cdot n_-} n_-$.

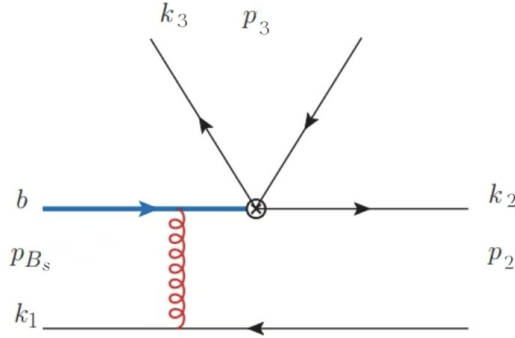


Figure 1: A LO diagram for the $\bar{B}_s(p_{B_s}) \rightarrow M_2(p_2)M_3(p_3)$ decay.

According to the conventions established in the referenced works [29, 36, 38], \bar{B}_s^0 meson WFs can be expressed as

$$\langle 0 | \bar{s}_\alpha(z) b_\beta(0) | \bar{B}_s^0(p) \rangle = \frac{f_{B_s}}{4N_c} \int d^4k e^{-ik_1 \cdot z} \left\{ (\not{p} + m_{B_s}) \gamma_5 \left[\frac{\not{n}_-}{\sqrt{2}} \phi_B^+ + \frac{\not{n}_+}{\sqrt{2}} \phi_B^- \right] \right\}_{\beta\alpha}. \quad (9)$$

In the above equation, f_{B_s} denotes the decay constant, $n_+ = (1, 0, 0)$ represents the positive direction, and $n_- = (0, 1, 0)$ corresponds to the negative direction. The scalar functions ϕ_B^+ and ϕ_B^- correspond to the leading and subleading twist WFs, respectively. These wave functions exhibit distinct asymptotic behaviors as the longitudinal momentum fraction of the light quark $x_1 \rightarrow 0$. Their relationship is given by the equation

$$\phi_B^+(x_1) + x_1 \phi_B^{-'}(x_1) = 0, \quad (10)$$

which reflects the equation of motion for the wave functions. We can define ϕ_{B1} and ϕ_{B2} based on the following relations

$$\phi_{B1} = \phi_B^+, \quad \phi_{B2} = \phi_B^+ - \phi_B^-. \quad (11)$$

Although the expressions for ϕ_B^+ and ϕ_B^- generally differ, the equation of motion (Eq. 10) often leads to the approximation $\phi_B^+ = \phi_B^-$ in many phenomenological studies of nonleptonic B meson decays. In this approximation, only the contributions from ϕ_{B1} are considered, and those from ϕ_{B2} are neglected. However, several studies [36, 37, 39–44] have demonstrated that ϕ_{B2} is not a negligible factor in HMEs, and its contributions to the form factor $F_0^{B \rightarrow \pi}$ in the PQCD approach can be as large as 30% in certain cases [40, 42]. Furthermore, the contribution of ϕ_{B2} to the branching ratio can be comparable to that from next-to-leading-order (NLO) corrections [36, 37]. This paper focuses on the potential influence of ϕ_{B2} in $B_s \rightarrow PP$ and PV decays within the PQCD framework. One commonly used expression for the leading B_s mesonic wave function ϕ_B^+ in actual PQCD calculations is given by [45],

$$\phi_B^+(x_1, b_1) = N x_1^2 \bar{x}_1^2 \exp \left\{ - \left(\frac{x_1 m_{B_s}}{\sqrt{2} \omega_{B_s}} \right)^2 - \frac{1}{2} \omega_{B_s}^2 b_1^2 \right\}. \quad (12)$$

The corresponding B_s mesonic WFs ϕ_B^- is written as [36, 40],

$$\begin{aligned} \phi_B^-(x_1, b_1) = N \frac{2 \omega_{B_s}^4}{m_{B_s}^4} \exp \left(- \frac{1}{2} \omega_{B_s}^2 b_1^2 \right) & \left\{ \sqrt{\pi} \frac{m_{B_s}}{\sqrt{2} \omega_{B_s}} \text{Erf} \left(\frac{m_{B_s}}{\sqrt{2} \omega_{B_s}}, \frac{x_1 m_{B_s}}{\sqrt{2} \omega_{B_s}} \right) \right. \\ & \left. + \left[1 + \left(\frac{m_{B_s} \bar{x}_1}{\sqrt{2} \omega_{B_s}} \right)^2 \right] \exp \left[- \left(\frac{x_1 m_{B_s}}{\sqrt{2} \omega_{B_s}} \right)^2 \right] - \exp \left(- \frac{m_{B_s}^2}{2 \omega_{B_s}^2} \right) \right\}. \end{aligned} \quad (13)$$

Here, ω_{B_s} denotes the shape parameter, and $\bar{x}_1 = 1 - x_1$. The normalization constant N_{B_s} is determined by the condition,

$$\int_0^1 dx_1 \phi_B^\pm(x_1, 0) = 1, \quad (14)$$

which ensures that the wave function is properly normalized. The shapes of the B_s meson DAs, including ϕ_B^+ and ϕ_B^- are illustrated in Fig. 2.

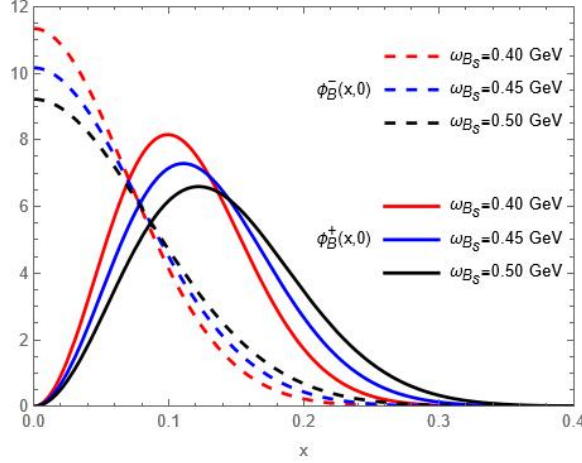


Figure 2: The shapes of the B_s DAs (ϕ_B^+ and ϕ_B^-) as a function of the longitudinal momentum fraction x (horizontal axis)

The following key observations can be made:

- The nonzero distributions of ϕ_B^\pm are predominantly located in the small x region, and ϕ_B^\pm vanishes as $x \rightarrow 1$. This is consistent with the expectation that the light quark in the B -meson carries a small longitudinal momentum fraction.
- The shapes of ϕ_B^- and ϕ_B^+ exhibit notable differences in the small x region. Particularly, the DAs ϕ_B^- and ϕ_B^+ show distinct endpoint behaviors at $x = 0$. This indicates that $\phi_{B2} = \phi_B^+ - \phi_B^- \neq 0$, suggesting that the approximation $\phi_{B2} = 0$ used in previous studies may be inappropriate and insufficient.
- Both ϕ_B^- and ϕ_{B2} are nonzero at the endpoint $x = 0$, resulting in an infrared divergence in the integral $\int \frac{dx}{x} \phi_{B2}$ under the collinear approximation. This suggests that the PQCD approach must account for nonperturbative contributions, potentially by considering the effects of the transverse momentum of the valence quarks and the inclusion of Sudakov factors.
- The distributions of ϕ_B^\pm are sensitive to the shape parameter ω_{B_s} . As ω_{B_s} increases, the distributions of ϕ_B^\pm become broader. Consequently, the theoretical results with the PQCD framework depend on the chosen value of ω_{B_s} .

The WFs for the final states, including light pseudoscalar mesons and longitudinally polarized vector mesons, are defined as follows [38, 46–48],

$$\langle P(p_2) | \bar{q}_i(0) q_j(z) | 0 \rangle$$

$$= -i \frac{f_P}{4N_c} \int_0^1 dx_2 e^{+ik_2 \cdot z} \left\{ \gamma_5 \left[\not{x}_2 \phi_P^a + \mu_P \phi_P^p - \mu_P (\not{x}_- \not{x}_+ - 1) \phi_P^t \right] \right\}_{ji}, \quad (15)$$

$$\begin{aligned} & \langle V(p_3, e_{\parallel}) | \bar{q}_i(0) q_j(z) | 0 \rangle \\ &= \frac{1}{4N_c} \int_0^1 dx_3 e^{+ik_3 \cdot z} \left\{ \not{\epsilon}_{\parallel} m_V f_V^{\parallel} \phi_V^v + \not{\epsilon}_{\parallel} \not{x}_3 f_V^{\perp} \phi_V^t - m_V f_V^{\perp} \phi_V^s \right\}_{ji}, \end{aligned} \quad (16)$$

In this context, f_P , f_V^{\parallel} , and f_V^{\perp} denote the decay constants. The wave functions ϕ_P^a and ϕ_V^v represent the twist-2 components, while $\phi_P^{p,t}$ and $\phi_V^{t,s}$ correspond to the twist-3 components.

Following the conventions outlined in Refs.[38, 47] and the DAs for the pseudoscalar meson $P = \pi, K$ meson are expressed as follows.

$$\phi_P^a(x) = 6x\bar{x} \{1 + a_1^P C_1^{3/2}(\xi) + a_2^P C_2^{3/2}(\xi)\}, \quad (17)$$

$$\begin{aligned} \phi_P^p(x) &= 1 + 3\rho_+^P - 9\rho_-^P a_1^P + 18\rho_+^P a_2^P \\ &\quad + \frac{3}{2}(\rho_+^P + \rho_-^P)(1 - 3a_1^P + 6a_2^P) \ln(x) \\ &\quad + \frac{3}{2}(\rho_+^P - \rho_-^P)(1 + 3a_1^P + 6a_2^P) \ln(\bar{x}) \\ &\quad - \left(\frac{3}{2}\rho_-^P - \frac{27}{2}\rho_+^P a_1^P + 27\rho_-^P a_2^P\right) C_1^{1/2}(\xi) \\ &\quad + (30\eta_p - 3\rho_-^P a_1^P + 15\rho_+^P a_2^P) C_2^{1/2}(\xi), \end{aligned} \quad (18)$$

$$\begin{aligned} \phi_P^t(x) &= \frac{3}{2}(\rho_-^P - 3\rho_+^P a_1^P + 6\rho_-^P a_2^P) \\ &\quad - C_1^{1/2}(\xi) \{1 + 3\rho_+^P - 12\rho_-^P a_1^P + 24\rho_+^P a_2^P \\ &\quad + \frac{3}{2}(\rho_+^P + \rho_-^P)(1 - 3a_1^P + 6a_2^P) \ln(x) \\ &\quad + \frac{3}{2}(\rho_+^P - \rho_-^P)(1 + 3a_1^P + 6a_2^P) \ln(\bar{x}) \\ &\quad - 3(3\rho_+^P a_1^P - \frac{15}{2}\rho_-^P a_2^P) C_1^{1/2}(\xi)\}. \end{aligned} \quad (19)$$

Similarly, the DAs for the vector mesons are given by the following expressions

$$\phi_V^v(x) = 6x\bar{x} \left\{ 1 + a_1^{\parallel,V} C_1^{3/2}(\xi) + a_2^{\parallel,V} C_2^{3/2}(\xi) \right\}, \quad (20)$$

$$\begin{aligned}
\phi_V^t(x) = & 3\xi\{C_1^{1/2}(\xi) + a_1^{\perp,V}C_2^{1/2}(\xi) + a_2^{\perp,V}C_3^{1/2}(\xi)\} \\
& + \frac{3}{2}\frac{m_s + m_q}{m_V}\frac{f_V^{\parallel}}{f_V^{\perp}}\{1 + 8\xi a_1^{\parallel,V} + (21 - 90x\bar{x})a_2^{\parallel,V} \\
& + \xi \ln \bar{x}(1 + 3a_1^{\parallel,V} + 6a_2^{\parallel,V}) - \xi \ln x(1 - 3a_1^{\parallel,V} + 6a_2^{\parallel,V})\} \\
& - \frac{3}{2}\frac{m_s - m_q}{m_V}\frac{f_V^{\parallel}}{f_V^{\perp}}\xi\{2 + 9\xi a_1^{\parallel,V} + (22 - 60x\bar{x})a_2^{\parallel,V} \\
& + \ln \bar{x}(1 + 3a_1^{\parallel,V} + 6a_2^{\parallel,V}) + \ln x(1 - 3a_1^{\parallel,V} + 6a_2^{\parallel,V})\}, \tag{21}
\end{aligned}$$

$$\begin{aligned}
\phi_V^s(x) = & \{-3C_1^{1/2}(\xi) - 3C_2^{1/2}(\xi)a_1^{\perp,V} - 3C_3^{1/2}(\xi)a_2^{\perp,V}\} \\
& - \frac{3}{2}\frac{m_s + m_q}{m_V}\frac{f_V^{\parallel}}{f_V^{\perp}}\{C_1^{1/2}(\xi) + 2C_2^{1/2}(\xi)a_1^{\parallel,V} \\
& + [3C_3^{1/2}(\xi) + 18C_1^{1/2}(\xi)]a_2^{\parallel,V} \\
& + (\ln \bar{x} + 1)(1 + 3a_1^{\parallel,V} + 6a_2^{\parallel,V}) \\
& - (\ln x + 1)(1 - 3a_1^{\parallel,V} + 6a_2^{\parallel,V})\} \\
& + \frac{3}{2}\frac{m_s - m_q}{m_V}\frac{f_V^{\parallel}}{f_V^{\perp}}\{9C_1^{1/2}(\xi)a_1^{\parallel,V} + 10C_2^{1/2}(\xi)a_2^{\parallel,V} \\
& + (\ln \bar{x} + 1)(1 + 3a_1^{\parallel,V} + 6a_2^{\parallel,V}) \\
& + (\ln x + 1)(1 - 3a_1^{\parallel,V} + 6a_2^{\parallel,V})\}. \tag{22}
\end{aligned}$$

In previous studies [36, 37], the effects of higher-order Gegenbauer polynomial terms - particularly those containing the third-order $C_3^m(\xi)$ (which were only partially included) and the fourth-order $C_4^m(\xi)$ polynomials - were not fully accounted for. To address this limitation, we systematically incorporate these higher-order contributions in our current framework. Following Refs.[38, 47], we introduce modified wave functions (denoted with a prime) that extend the original formulations through the inclusion of additional terms derived from the complete set of higher-order Gegenbauer polynomials.

$$\phi_P^{a'}(x) = \phi_P^a(x) + 6x\bar{x}\{a_4^P C_4^{3/2}(\xi)\}, \tag{23}$$

$$\phi_P^{p'}(x) = \phi_P^p(x) + (10\eta_P\lambda_{3P} - \frac{9}{2}\rho_-^p a_2^p)C_3^{1/2}(\xi) - 3\eta_P\omega_{3P}C_4^{1/2}(\xi), \quad (24)$$

$$\phi_P^{t'}(x) = \phi_P^t(x) - (5\eta_P - \frac{1}{2}\eta_P\omega_{3P} + \frac{3}{2}\rho_+^K a_2^K)C_3^{1/2} - \frac{5}{3}\eta_P\lambda_{3P}C_4^{1/2}, \quad (25)$$

$$\phi_V^{v'}(x) = \phi_V^v(x) + 6x\bar{x} \left\{ a_4^{\parallel,V} C_4^{3/2}(\xi) \right\}, \quad (26)$$

$$\phi_V^{t'}(x) = \phi_V^t(x) + (15\kappa_{3V}^\perp - \frac{3}{2}\lambda_{3V}^\perp)C_3^{1/2}(\xi) + 5\omega_{3V}^\perp C_4^{1/2}(\xi), \quad (27)$$

$$\phi_V^{s'}(x) = \phi_V^s(x) + \{-15C_2^{1/2}(\xi)\kappa_{3V}^\perp - C_3^{1/2}(\xi)\omega_{3V}^\perp\} + \frac{1}{4}\lambda_{3V}^\perp C_4^{1/2}(\xi). \quad (28)$$

Here, $\xi = x - \bar{x} = 2x - 1$, $\rho_+^P = \frac{M_P^2}{\mu_P^2}$, $\eta_P = \frac{f_{3P}}{f_P\mu_P}$. C_n^m represents the Gegenbauer polynomials. a_n^P , $a_n^{\parallel,V}$ and a_n^\perp are the corresponding the Gegenbauer moments.

We present the DA curves for the π , K , and K^* mesons as examples, shown in Fig.3. From the figure, it is evident that higher-order terms influence the DAs; however, the exact extent of this effect requires further calculation.

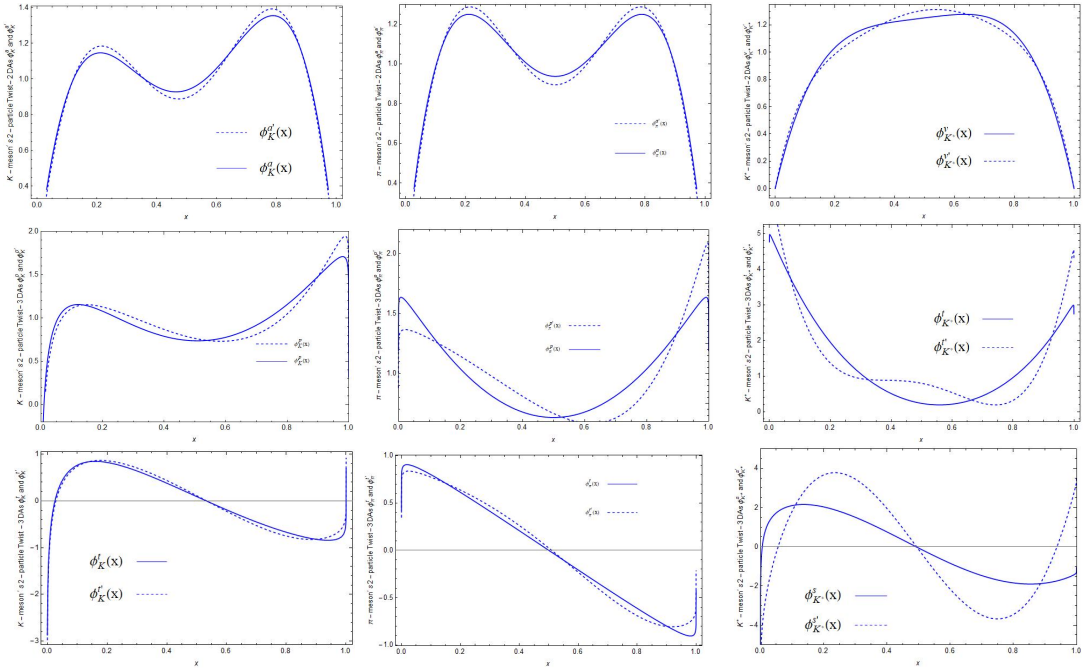


Figure 3: Shape lines of the final meson DAs, with (solid lines) and without (dotted lines) higher-order Gegenbauer polynomials, as a function of the longitudinal momentum fraction x .

Table 2: Summary of theoretical input parameters, with the central values taken as the default.

Wolfenstein parameters of the CKM matrix [5]			
$A = 0.826^{+0.016}_{-0.015}$	$\lambda = 0.22501 \pm 0.00068$	$\bar{\rho} = 0.1591 \pm 0.0094$	$\bar{\eta} = 0.3523^{+0.0073}_{-0.0071}$
mass of particle (in the unit of MeV) [5] (MeV)			
$m_{\pi^\pm} = 139.57$	$m_{K^\pm} = 493.677 \pm 0.015$	$m_\rho = 775.26 \pm 0.23$	$m_{K^{*\pm}} = 895.5 \pm 0.8$
$m_{\pi^0} = 134.98$	$m_{K^0} = 497.611 \pm 0.013$	$m_\omega = 782.66 \pm 0.13$	$m_{K^{*0}} = 895.55 \pm 0.20$
$m_b = 4780 \pm 6$	$m_\phi = 1019.461 \pm 0.016$	$m_{B_s} = 5366.93 \pm 0.10$	
decay constants (in the unit of MeV) and lifetime [47]			
$f_\rho^\parallel = 216 \pm 3$	$f_\omega^\parallel = 187 \pm 5$	$f_\phi^\parallel = 215 \pm 5$	$f_{K^*}^\parallel = 220 \pm 5$
$f_\rho^\perp = 165 \pm 9$	$f_\omega^\perp = 151 \pm 9$	$f_\phi^\perp = 186 \pm 9$	$f_{K^*}^\perp = 185 \pm 10$
$f_{B_s} = 230.3 \pm 1.3[5]$	$f_\pi = 130.2 \pm 0.8[5]$	$f_K = 155.7 \pm 0.3[5]$	$\tau_{B_s^0} = 1.51 \text{ ps}$
Gegenbauer moments at the scale of $\mu = 1 \text{ GeV}$ [38, 47]			
$a_1^{\pi(\rho)} = a_1^{\omega(\phi)} = 0$	$a_2^\pi = 0.25 \pm 0.15$	$a_1^K = 0.06 \pm 0.03$	$a_2^K = 0.25 \pm 0.15$
$a_2^{\parallel, \rho(\omega)} = 0.15 \pm 0.07$	$a_2^{\parallel, \phi} = 0.18 \pm 0.08$	$a_1^{\parallel, K^*} = 0.03 \pm 0.02$	$a_2^{\parallel, K^*} = 0.11 \pm 0.09$
$a_2^{\perp, \rho(\omega)} = 0.14 \pm 0.06$	$a_2^{\perp, \phi} = 0.14 \pm 0.07$	$a_1^{\perp, K^*} = 0.04 \pm 0.03$	$a_2^{\perp, K^*} = 0.10 \pm 0.08$
$a_4^{\rho(\omega)} = 0.03 \pm 0.02$	$a_4^\phi = 0.02^{+0.01}_{-0.02}$	$a_4^{K^*} = 0.02 \pm 0.01$	$a_4^{\pi, K} = -0.015$

4 Numerical analysis

The Feynman diagrams governing two-body nonleptonic B_s meson decays are illustrated in Fig.4. Within the pQCD framework, the decay amplitude \mathcal{A} is systematically factorized into three essential components: (i) short-distance Wilson coefficients C_i encoding electroweak-scale dynamics, (ii) hard scattering kernels \mathcal{H}_i describing quark-level interactions, and (iii) hadronic wave functions Φ_i parametrizing non-perturbative bound-state effects. The generalized amplitude structure can be expressed as

$$\mathcal{A}_i \propto \int \prod_j dx_j db_j C_i(t_i) \mathcal{H}_i(t_i, x_j, b_j) \Phi_j(x_j, b_j) e^{-S_j}. \quad (29)$$

In the rest frame of the B_s meson, the CP -averaged branching ratio is formally expressed as

$$\mathcal{B}(B_s \rightarrow PP) = \frac{\tau_{B_s}}{16\pi} \frac{p_{\text{cm}}}{m_{B_s}^2} \{ |\mathcal{A}(B_s \rightarrow f)|^2 + |\mathcal{A}(\bar{B}_s \rightarrow \bar{f})|^2 \}, \quad (30)$$

$$\mathcal{B}(B_s \rightarrow PV) = \frac{\tau_{B_s}}{16\pi} \frac{p_{\text{cm}}^3}{m_V^2} \frac{|\mathcal{A}(B_s \rightarrow f)|^2 + |\mathcal{A}(\bar{B}_s \rightarrow \bar{f})|^2}{(\epsilon \cdot p_{B_s})^2}, \quad (31)$$

where τ_{B_s} denotes the B_s -meson lifetime, $p_{\text{cm}} = \sqrt{\lambda(m_{B_s}^2, m_{M_1}^2, m_{M_2}^2)}/(2m_{B_s})$ is the magnitude of the three-momentum shared by the pseudoscalar (P) or vector (V) mesons in the final state, and the Källén function $\lambda(a, b, c) = a^2 + b^2 + c^2 - 2ab - 2ac - 2bc$. The explicit forms of the amplitudes, including ϕ_{B2} -dependent terms, are systematically derived in Appendix A.

The time-dependent CP -violating asymmetry for the neutral \bar{B}_s^0 meson decay into a final state f (with $f = \bar{f}$) is defined through the normalized decay rate difference:

$$\mathcal{A}_{CP} = \frac{\Gamma(\bar{B}_s^0 \rightarrow f) - \Gamma(B_s^0 \rightarrow \bar{f})}{\Gamma(\bar{B}_s^0 \rightarrow f) + \Gamma(B_s^0 \rightarrow \bar{f})}. \quad (32)$$

Notably, for the decay channel $\bar{B}_s^0 \rightarrow K^+\pi^-$, the final state $\bar{f} = K^+\pi^-$ is not a CP eigenstate. Consequently, the direct CP asymmetry is defined as

$$\mathcal{A}_{CP}(B_s^0 \rightarrow \pi^+ K^-) = \frac{|\bar{A}_{\bar{f}}|^2 - |A_f|^2}{|\bar{A}_{\bar{f}}|^2 + |A_f|^2}, \quad (33)$$

where A_f and $\bar{A}_{\bar{f}}$ denote the decay amplitudes for $B_s^0 \rightarrow f$ and $\bar{B}_s^0 \rightarrow \bar{f}$ processes, respectively.

As indicated in the reference [36], the selection of the parameter ω_{B_s} significantly influences the branching ratio calculations. To determine the optimal value of ω_{B_s} , we employed the least-squares method, which is commonly used in theoretical physics to minimize the sum of the squares of the differences between observed and calculated values.

The χ^2 statistic is defined as:

$$\chi^2 = \sum_i \chi_i^2 = \sum_i \frac{(\mathcal{B}_i^{\text{th}} - \mathcal{B}_i^{\text{exp}})^2}{\sigma_i^2}, \quad (34)$$

where $\mathcal{B}_i^{\text{th}}$ and $\mathcal{B}_i^{\text{exp}}$ represent the theoretical and experimental branching ratios for the i -th decay mode, respectively, and σ_i denotes the experimental uncertainty.

We performed calculations for the decays $\bar{B}_s^0 \rightarrow PP$ and PV using data from both PDG and LHCb. The resulting χ^2 distributions as functions of ω_{B_s} are presented in Figures 5 and 6 for the respective decay modes. The combined distribution, incorporating both decay processes, is shown in Figure 7. The fitting results obtained from both datasets exhibit close agreement. However, given the more comprehensive nature of the PDG data, we selected the optimal values of ω_{B_s} derived from these calculations for further analysis:

- For the decay $\bar{B}_s^0 \rightarrow PP$, we adopted $\omega_{B_s} = 0.49$ GeV.
- For the decay $\bar{B}_s^0 \rightarrow PV$, we selected $\omega_{B_s} = 0.45$ GeV.

- For the combined decay modes $\bar{B}_s^0 \rightarrow PP, PV$, we chose $\omega_{B_s} = 0.48$ GeV.

The numerical results for the branching ratios of the decay modes $\bar{B}_s^0 \rightarrow PP$ and PV are shown in Tables 3 and 4, respectively, while the direct CP violation results are presented in Table 5. Furthermore, a comparison between the branching ratios calculated with and without the inclusion of higher-order terms in the final-state meson DAs can be found in Table 6. The results obtained for $\omega_{B_s} = 0.48$ GeV are listed in Table 7, while the numerical results for the $\bar{B}_s^0 \rightarrow PV$ decay mode from previous studies and the experimental data provided by PDG and HFLAV are shown in Table 8.

From a comparison of the numerical results presented in the tables, we can draw the following conclusions:

- **Branching Ratios:** As indicated in Table 3, the branching ratio for the decay $B_s \rightarrow KK$ is generally larger than those for $B_s \rightarrow \pi K$ and $B_s \rightarrow \pi\pi$. For each decay channel, the inclusion of the contribution from ϕ_{B2} leads to a distinct enhancement in the branching ratio, particularly in certain decay channels (e.g., $\bar{B}_s^0 \rightarrow \pi^0 K^0$, $\bar{B}_s^0 \rightarrow K^- K^+$ and $\bar{B}_s^0 \rightarrow \bar{K}^0 K^0$), where the contribution from ϕ_{B2} can even reach the level of subleading corrections. This suggests that the impact of ϕ_{B2} cannot be neglected in precision calculations of B_s meson weak decays.
- **Larger Branching Ratios:** The larger branching ratios are observed for the decays $\bar{B}_s^0 \rightarrow K^- K^+$, $\bar{B}_s^0 \rightarrow \bar{K}^0 K^0$ and $\bar{B}_s^0 \rightarrow \rho^- K^+$. When both ϕ_{B1} and ϕ_{B2} contributions are considered, the branching ratios can reach magnitudes on the order of 10^{-5} , which are likely to be observed experimentally in the future.
- **Direct CP Violation:** Tables 5 indicate that the contribution of ϕ_{B2} to direct CP violation varies across different decay channels. For instance, in the decay $\bar{B}_s^0 \rightarrow K^- K^+$, the contribution of ϕ_{B2} is 13%, while in the decays $\bar{B}_s^0 \rightarrow \pi^+ \pi^-$ and $\bar{B}_s^0 \rightarrow \pi^0 \pi^0$, the contribution of ϕ_{B2} is nearly a factor of two larger. Experimentally, the direct CP violation in the decay $\bar{B}_s^0 \rightarrow \pi^- K^+$ is measured to be 0.224 ± 0.012 , and our calculated value is of the same order of magnitude. Since CP violation is closely related to strong phase shifts, obtaining precise information about these strong phases is essential for a more comprehensive understanding of CP violation phenomena. However, the factors influencing the strong phases, such as higher-order radiative corrections to hadronic matrix elements and final-state interactions between particles, complicate the analysis. Additionally, due to the lack of effective constraints on these factors, the experimental precision of CP violation measurements is often limited, resulting in a sizable discrepancy between theoretical predictions and experimental data.
- **Uncertainty Analysis:** The impact of various theoretical parameters on the branching ratio is discussed in Tables 3 and 4. Among the parameters, the Gegenbauer parameter, chiral masses,

and the wave function parameter ω_{B_s} exhibit significant effects, while the uncertainty due to the B_s meson decay constant is relatively small. The error due to variations in μ_P ranges from 5.0% to 32.0%, while the error due to changes in ω_{B_s} ranges from 2.8% to 20.0%. The error due to the Gegenbauer parameter is stable, typically between 7% and 10%, and the total theoretical uncertainty falls within the range of 9.2% to 33.5%. Given the sensitivity of the branching ratio to the wave function parameter ω_{B_s} , an appropriate choice of ω_{B_s} can enhance the contribution from ϕ_{B1} and partially compensate for the contribution from ϕ_{B2} . This may explain why the contribution from ϕ_{B2} has often been overlooked in previous studies. Overall, ϕ_{B2} does affect both the branching ratios and CP violation, and its contribution should not be ignored.

- **Higher-Order Terms:** As seen in Table 6, the inclusion of higher-order terms in the final-state meson DAs leads to changes in the branching ratio calculations. For example, the inclusion of higher-order terms in the decay $\bar{B}_s^0 \rightarrow \rho^0 K^0$ results in an impact on the branching ratio of up to 6%. Overall, within the allowed error range, our calculations are consistent with previous theoretical predictions, although the inclusion of higher-order terms and the different choices of parameters contribute to some deviations in the results.
- **Fitting with Multiple Decay Channels:** When both decay modes are considered simultaneously in the fit, the optimal value of ω_{B_s} is found to be 0.48 GeV, which is consistent with results from references [45, 49]. Using this optimal ω_{B_s} , we obtain the results presented in Table 7. Compared to previous calculations, we observe that the branching ratios for some decay modes increase with an increasing ω_{B_s} , while for others, they decrease. From a comprehensive analysis of all the tables, we infer that previous calculations likely selected an appropriate ω_{B_s} to minimize the discrepancy between theoretical predictions and experimental data. This suggests that the contribution from ϕ_{B2} may be effectively replaced by other input parameters, which could explain why the contribution from ϕ_{B2} has often been neglected in earlier studies.

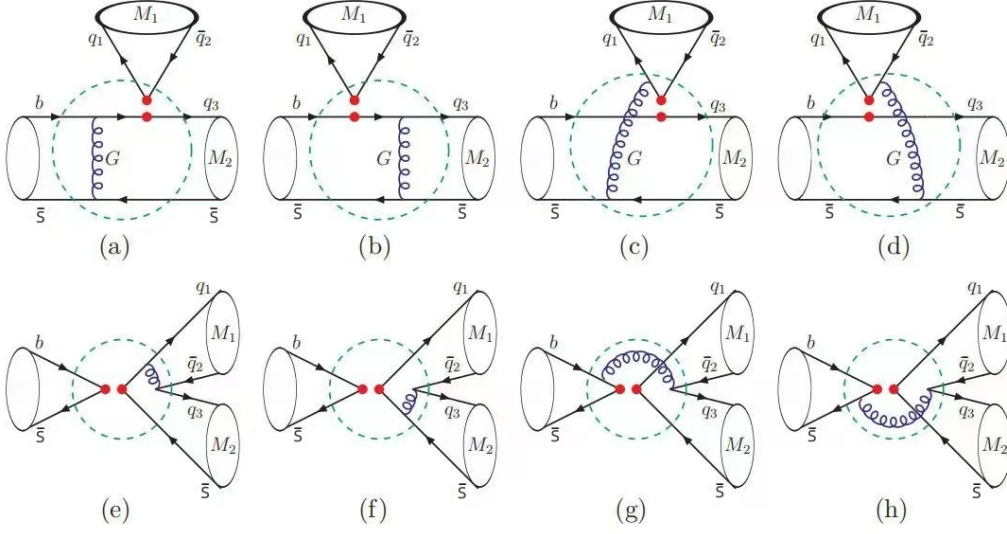


Figure 4: Feynman diagrams contributing to the $\bar{B}_s^0 \rightarrow M_1 M_2$ decay processes. Dots denote interaction vertices, while the dashed circles represent quark-level scattering amplitudes. Diagrams are categorized as follows: (a) and (b) factorizable emission diagrams; (c) and (d) nonfactorizable emission diagrams; (e) and (f) factorizable annihilation diagrams; (g) and (h) nonfactorizable annihilation diagrams.

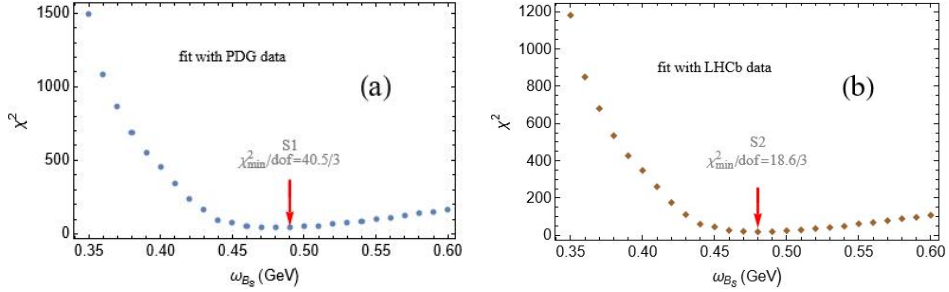


Figure 5: χ^2 distribution as a function of the B_s -meson shape parameter ω_{B_s} for the $\bar{B}_s^0 \rightarrow PP$ decay analysis. The global fit incorporates experimental constraints from $B_s \rightarrow PP$ measurements by PDG and LHCb. Red data points (marked by arrows) indicate the χ^2 minima, corresponding to the optimized ω_{B_s} values.

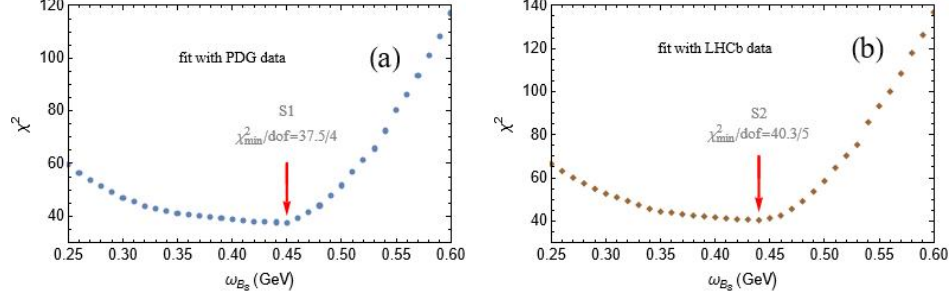


Figure 6: χ^2 distribution as a function of the B_s -meson shape parameter ω_{B_s} for the $\bar{B}_s^0 \rightarrow PV$ decay analysis. Other legends are the same as those of figure 5.

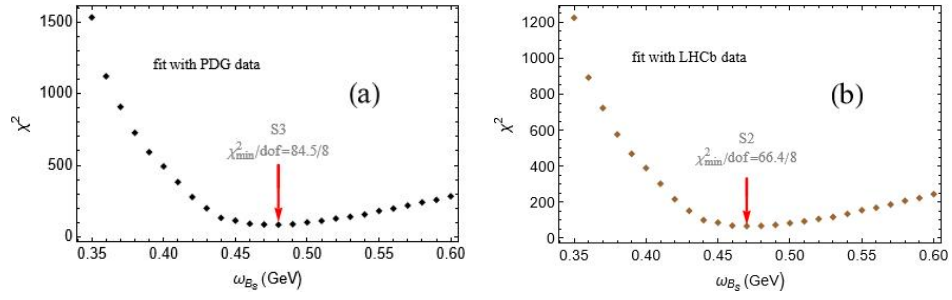


Figure 7: χ^2 distribution as a function of the B_s -meson shape parameter ω_{B_s} for both $\bar{B}_s^0 \rightarrow PP$ and PV decay analyses. Other legends are the same as those of figure 5.

Table 3: CP-averaged branching ratios (in units of 10^{-6}) for $\bar{B}_s^0 \rightarrow PP$ decays. For each decay channel, the first row corresponds to the results with $\phi_{B_2} = 0$, while the second row shows the case with $\phi_{B_2} \neq 0$. The systematic uncertainties in columns 3-6 are respectively induced by the Gegenbauer parameter $a_2^P = 0.25 \pm 0.15$, factorization scale $\mu_P = 1.4 \pm 0.1$ GeV, and B_s -meson shape parameter $\omega_{B_s} = 0.49 \pm 0.01$ GeV and decay constant $f_{B_s} = 230.3 \pm 1.3$ MeV (see Table 2 for other input parameters).

mode	Center value	a_2^P	μ_P	ω_{B_s}	f_{B_s}	total
$\bar{B}_s^0 \rightarrow \pi^- K^+$	6.599	+0.572 -0.495	+0.756 -0.562	+0.485 -0.436	+0.128 -0.127	+1.073 -0.876
	8.639	+0.453 -0.397	+0.880 -0.692	+0.242 -0.307	+0.104 -0.121	+1.102 -0.863
$\bar{B}_s^0 \rightarrow \pi^- \pi^+$	0.634	+0.055 -0.050	+0.166 -0.109	+0.102 -0.029	+0.033 -0.032	+0.205 -0.127
	0.958	+0.096 -0.085	+0.134 -0.127	+0.091 -0.063	+0.054 -0.051	+0.196 -0.173
$\bar{B}_s^0 \rightarrow \pi^0 K^0$	0.170	+0.012 -0.014	+0.021 -0.024	+0.008 -0.009	+0.007 -0.007	+0.026 -0.030
	0.260	+0.022 -0.021	+0.040 -0.044	+0.046 -0.052	+0.010 -0.010	+0.066 -0.072
$\bar{B}_s^0 \rightarrow K^- K^+$	12.997	+1.134 -1.212	+3.088 -3.559	+0.130 -1.506	+0.062 -0.089	+3.293 -4.051
	19.040	+1.327 -1.458	+3.930 -4.423	+1.604 -2.708	+0.429 -0.424	+4.468 -5.404
$\bar{B}_s^0 \rightarrow K^0 \bar{K}^0$	15.190	+1.394 -1.411	+2.032 -1.970	+0.93 -1.648	+0.349 -0.342	+2.657 -2.950
	18.502	+1.653 -1.582	+1.984 -1.887	+1.064 -2.092	+0.427 -0.416	+2.825 -3.258
$\bar{B}_s^0 \rightarrow \pi^0 \pi^0$	0.317	+0.028 -0.025	+0.083 -0.055	+0.051 -0.014	+0.017 -0.016	+0.103 -0.064
	0.479	+0.045 -0.039	+0.067 -0.064	+0.048 -0.031	+0.027 -0.026	+0.098 -0.085

Table 4: CP-averaged branching ratios (in units of 10^{-6}) for $\bar{B}_s^0 \rightarrow PV$ decays, B_s -meson shape parameter $\omega_{B_s} = 0.45 \pm 0.01$ GeV. Other notations and theoretical error conventions follow Table 3 .

mode	Center value	a_2^P	μ_P	ω_{B_s}	f_{B_s}	total
$\bar{B}_s^0 \rightarrow \rho^0 K^0$	0.088	+0.007 -0.007	+0.007 -0.006	+0.013 -0.008	+0.004 -0.004	+0.017 -0.013
	0.089	+0.007 -0.008	+0.009 -0.008	+0.013 -0.007	+0.004 -0.004	+0.018 -0.014
$\bar{B}_s^0 \rightarrow \pi^0 K^{*0}$	0.108	+0.009 -0.009	+0.007 -0.008	+0.002 -0.003	+0.001 -0.002	+0.012 -0.013
	0.126	+0.011 -0.012	+0.009 -0.009	+0.003 -0.003	+0.001 -0.002	+0.015 -0.015
$\bar{B}_s^0 \rightarrow \omega K^0$	0.106	+0.008 -0.008	+0.025 -0.025	+0.013 -0.013	+0.009 -0.008	+0.031 -0.030
	0.169	+0.014 -0.013	+0.027 -0.029	+0.017 -0.019	+0.010 -0.009	+0.036 -0.038
$\bar{B}_s^0 \rightarrow K^0 \phi$	0.153	+0.013 -0.011	+0.011 -0.016	+0.001 -0.001	+0.005 -0.005	+0.018 -0.020
	0.147	+0.012 -0.011	+0.010 -0.015	+0.001 -0.001	+0.006 -0.006	+0.017 -0.020
$\bar{B}_s^0 \rightarrow K^{*-} K^+$	8.196	+0.725 -0.694	+0.433 -0.427	+0.224 -0.235	+0.104 -0.091	+0.880 -0.853
	11.996	+1.125 -1.096	+0.551 -0.425	+0.331 -0.337	+0.137 -0.164	+1.303 -1.234
$\bar{B}_s^0 \rightarrow K^- K^{*+}$	4.889	+0.339 -0.280	+0.333 -0.314	+0.199 -0.156	+0.014 -0.019	+0.515 -0.449
	7.584	+0.692 -0.734	+0.538 -0.561	+0.352 -0.307	+0.021 -0.023	+0.945 -0.974
$\bar{B}_s^0 \rightarrow \bar{K}^{*0} K^0$	6.808	+0.492 -0.453	+0.550 -0.562	+1.088 -0.546	+0.021 -0.021	+1.315 -0.905
	9.832	+0.877 -0.892	+0.866 -0.887	+1.709 -1.415	+0.025 -0.025	+2.107 -1.893
$\bar{B}_s^0 \rightarrow \bar{K}^0 K^{*0}$	5.480	+0.433 -0.398	+0.830 -1.135	+0.330 -0.352	+0.017 -0.020	+0.993 -1.253
	6.626	+0.635 -0.593	+1.648 -2.123	+0.271 -0.293	+0.023 -0.023	+1.787 -2.224
$\bar{B}_s^0 \rightarrow \pi^- K^{*+}$	6.890	+0.580 -0.623	+0.376 -0.275	+0.407 -0.438	+0.015 -0.014	+0.802 -0.810
	7.782	+0.745 -0.690	+0.125 -0.129	+0.406 -0.486	+0.010 -0.015	+0.858 -0.854
$\bar{B}_s^0 \rightarrow \rho^- K^+$	16.966	+1.156 -1.253	+1.014 -1.015	+1.117 -1.103	+0.229 -0.171	+1.914 -1.961
	17.207	+1.359 -1.420	+1.024 -1.025	+1.414 -1.118	+0.246 -0.209	+2.226 -2.088

Table 5: The CP asymmetries \mathcal{A}_{CP} (in the unit of 10^{-2}) for the $\bar{B}_s^0 \rightarrow PP$ and $\bar{B}_s^0 \rightarrow PV$ decays. Notations and theoretical error conventions follow Tables 3 and 4.

mode	Center value	a_2^P	μ_P	ω_{B_s}	f_{B_s}	total
$\bar{B}_s^0 \rightarrow \pi^- K^+$	18.325	+2.337 -2.341	+0.626 -0.429	+0.069 -1.018	+0.056 -0.057	+2.421 -2.589
	16.232	+2.159 -2.163	+0.504 -2.433	+0.421 -0.626	+0.011 -0.009	+2.257 -3.315
$\bar{B}_s^0 \rightarrow \pi^- \pi^+$	-0.917	+0.374 -0.376	+0.056 -0.057	+0.199 -0.014	—	+0.427 -0.381
	-1.776	+0.382 -0.383	+0.015 -0.016	+0.167 -0.009	—	+0.417 -0.383
$\bar{B}_s^0 \rightarrow \pi^0 K^0$	32.089	+4.492 -4.263	+0.575 -0.364	+0.992 -0.942	—	+4.636 -4.381
	42.858	+4.936 -4.749	+1.066 -0.870	+1.853 -0.889	—	+5.764 -5.373
$\bar{B}_s^0 \rightarrow K^- K^+$	-4.808	+1.236 -1.597	+0.425 -0.230	+0.717 -0.566	+0.003 -0.002	+1.509 -1.725
	-4.179	+1.327 -1.458	+0.875 -0.428	+0.535 -0.449	+0.002 -0.001	+2.016 -2.089
$\bar{B}_s^0 \rightarrow \pi^0 \pi^0$	-0.917	+0.374 -0.376	+0.056 -0.067	+0.199 -0.014	—	+0.429 -0.382
	-1.776	+0.382 -0.383	+0.015 -0.016	+0.167 -0.009	—	+0.421 -0.388
$\bar{B}_s^0 \rightarrow \rho^0 K^0$	71.748	+9.334 -5.298	+7.859 -2.326	+0.200 -0.061	+0.046 -0.012	+12.204 -5.786
	70.823	+8.276 -5.131	+8.468 -2.050	+0.205 -0.068	+0.020 -0.013	+11.842 -5.526
$\bar{B}_s^0 \rightarrow \pi^0 K^{*0}$	-26.540	+5.359 -5.363	+4.248 -1.599	+0.549 -2.517	+0.187 -0.283	+6.863 -6.143
	-37.735	+6.286 -6.763	+5.655 -2.315	+1.564 -4.052	+0.166 -0.315	+8.600 -8.223
$\bar{B}_s^0 \rightarrow \omega K^0$	33.740	+3.798 -4.039	+1.435 -1.786	+4.563 -5.599	+0.165 -0.155	+6.110 -7.133
	46.638	+5.296 -5.557	+0.078 -0.066	+3.877 -5.415	+0.177 -0.169	+6.566 -7.761
$\bar{B}_s^0 \rightarrow K^{*-} K^+$	-17.482	+2.235 -2.649	+0.340 -0.429	+0.384 -0.238	+0.098 -0.042	+2.295 -2.694
	-12.551	+2.012 -2.253	+0.325 -0.446	+1.083 -0.446	+0.031 -0.020	+2.308 -2.340
$\bar{B}_s^0 \rightarrow K^- K^{*+}$	10.586	+7.253 -7.379	+5.181 -6.836	+0.340 -0.429	+0.069 -0.026	+8.920 -10.068
	8.948	+6.203 -6.346	+0.282 -0.986	+0.326 -0.407	+0.046 -0.073	+6.218 -6.435
$\bar{B}_s^0 \rightarrow \pi^- K^{*+}$	5.774	+2.737 -2.752	+2.145 -1.414	+0.693 -0.696	+0.175 -0.183	+3.550 -3.177
	-2.051	+1.839 -1.846	+1.718 -0.756	+0.918 -0.915	+0.195 -0.207	+2.686 -2.204
$\bar{B}_s^0 \rightarrow \rho^- K^+$	-34.159	+4.460 -4.393	+2.857 -2.958	+0.085 -0.068	+0.022 -0.015	+5.297 -5.297
	-35.164	+5.285 -5.326	+3.521 -3.506	+0.024 -0.048	+0.009 -0.003	+6.351 -6.377

Table 6: Comparison of branching ratio (in the unit of 10^{-6}) results after incorporating higher-order terms into the final-state meson DAs. Symbols ϕ'_{B1} and ϕ'_{B2} denote predictions including these corrections, while ω_{B_s} is set to 0.49 GeV for PP and 0.45 GeV for PV .

Mode	$\bar{B}_s^0 \rightarrow \pi^- K^+$		$\bar{B}_s^0 \rightarrow \pi^+ \pi^-$		$\bar{B}_s^0 \rightarrow \pi^0 K^0$		$\bar{B}_s^0 \rightarrow K^- K^+$	
$\phi_{B1}/\phi_{B1'}$	6.599	6.738	0.634	0.652	0.170	0.175	12.997	12.744
$\phi_{B2}/\phi_{B2'}$	8.639	8.971	0.958	1.009	0.260	0.273	19.040	18.589
Mode	$\bar{B}_s^0 \rightarrow \bar{K}^0 K^0$		$\bar{B}_s^0 \rightarrow \pi^0 \pi^0$		$\bar{B}_s^0 \rightarrow \rho^0 K^0$		$\bar{B}_s^0 \rightarrow \pi^0 K^{*0}$	
$\phi_{B1}/\phi_{B1'}$	15.190	15.305	0.317	0.326	0.088	0.082	0.108	0.109
$\phi_{B2}/\phi_{B2'}$	18.502	18.669	0.479	0.505	0.089	0.083	0.126	0.120
Mode	$\bar{B}_s^0 \rightarrow \omega K^0$		$\bar{B}_s^0 \rightarrow K^0 \phi$		$\bar{B}_s^0 \rightarrow K^{*-} K^+$		$\bar{B}_s^0 \rightarrow K^- K^{*+}$	
$\phi_{B1}/\phi_{B1'}$	0.106	0.109	0.153	0.160	8.196	8.562	4.889	5.134
$\phi_{B2}/\phi_{B2'}$	0.169	0.174	0.147	0.149	11.996	12.531	7.584	7.815
Mode	$\bar{B}_s^0 \rightarrow \bar{K}^{*0} K^0$		$\bar{B}_s^0 \rightarrow \bar{K}^0 K^{*0}$		$\bar{B}_s^0 \rightarrow \pi^- K^{*+}$		$\bar{B}_s^0 \rightarrow \rho^- K^+$	
$\phi_{B1}/\phi_{B1'}$	6.808	7.049	5.480	5.673	6.890	7.128	16.966	17.175
$\phi_{B2}/\phi_{B2'}$	9.832	10.116	6.626	7.039	7.782	8.226	17.207	18.026

Table 7: Branching ratios (in units of 10^{-6}) for the $\bar{B}_s^0 \rightarrow PP, PV$ decays with $\omega_{B_s} = 0.48\text{GeV}$.

Mode	$\bar{B}_s^0 \rightarrow \pi^- K^+$	$\bar{B}_s^0 \rightarrow \pi^+ \pi^-$	$\bar{B}_s^0 \rightarrow \pi^0 K^0$	$\bar{B}_s^0 \rightarrow K^- K^+$
$\phi_{B1} + \phi_{B2}$	8.881	1.049	0.306	20.644
ϕ_{B1}	7.084	0.736	0.178	13.127
Mode	$\bar{B}_s^0 \rightarrow \bar{K}^0 K^0$	$\bar{B}_s^0 \rightarrow \pi^0 \pi^0$	$\bar{B}_s^0 \rightarrow \rho^0 K^0$	$\bar{B}_s^0 \rightarrow \pi^0 K^{*0}$
$\phi_{B1} + \phi_{B2}$	19.566	0.525	0.085	0.113
ϕ_{B1}	16.120	0.368	0.084	0.103
Mode	$\bar{B}_s^0 \rightarrow \omega K^0$	$\bar{B}_s^0 \rightarrow K^0 \phi$	$\bar{B}_s^0 \rightarrow K^{*-} K^+$	$\bar{B}_s^0 \rightarrow K^- K^{*+}$
$\phi_{B1} + \phi_{B2}$	0.204	0.143	12.927	8.589
ϕ_{B1}	0.127	0.150	8.853	5.474
Mode	$\bar{B}_s^0 \rightarrow \bar{K}^{*0} K^0$	$\bar{B}_s^0 \rightarrow \bar{K}^0 K^{*0}$	$\bar{B}_s^0 \rightarrow \pi^- K^{*+}$	$\bar{B}_s^0 \rightarrow \rho^- K^+$
$\phi_{B1} + \phi_{B2}$	10.736	7.089	9.132	14.136
ϕ_{B1}	7.573	5.863	8.036	13.938

Table 8: Comparison of theoretical predictions with experimental measurements for $\bar{B}_s^0 \rightarrow PP, PV$ decays. The presented results include pQCD calculations at LO[29, 32, 33, 50] and NLO[32, 33, 50] accuracy, QCDF[23, 29] predictions, and available experimental data from PDG[5] and HFLAV[22].

mode	pQCD _{LO} [29, 32, 33, 50]			pQCD _{NLO} [32, 33, 50]		QCDF[23, 29]	PDG[5]	HFLAV[22]
$\bar{B}_s^0 \rightarrow \pi^- K^+$	$7.6^{+3.3}_{-2.5}$	6.9	7.0	$5.70^{+2.3}_{-1.5}$	$5.4^{+2.4}_{-1.5}$	10.2	5.9 ± 0.7	$6.1^{+0.9}_{-0.8}$
$\bar{B}_s^0 \rightarrow \pi^+ \pi^-$	$0.57^{+0.18}_{-0.16}$	0.62	0.70	$0.57^{+0.24}_{-0.22}$	$0.52^{+0.21}_{-0.18}$	0.024	0.72 ± 0.1	$0.74^{+0.12}_{-0.10}$
$\bar{B}_s^0 \rightarrow \pi^0 K^0$	$0.16^{+0.12}_{-0.07}$	0.18	0.16	$0.28^{+0.10}_{-0.08}$	$0.27^{+0.10}_{-0.08}$	0.49	—	—
$\bar{B}_s^0 \rightarrow K^- K^+$	$13.6^{+8.6}_{-5.2}$	13.4	11.8	$19.7^{+6.6}_{-5.7}$	$18.6^{+6.4}_{-5.3}$	22.7	27.2 ± 2.3	$27.4^{+3.2}_{-2.8}$
$\bar{B}_s^0 \rightarrow \bar{K}^0 K^0$	$15.6^{+9.7}_{-6.0}$	14.4	14.3	$20.2^{+7.3}_{-5.8}$	$19.7^{+5.9}_{-3.8}$	24.7	17.6 ± 3.1	17.4 ± 3.1
$\bar{B}_s^0 \rightarrow \pi^0 \pi^0$	$0.28^{+0.09}_{-0.08}$	0.25	0.35	$0.29^{+0.12}_{-0.12}$	$0.21^{+0.10}_{-0.09}$	0.012	< 7.7	—
$\bar{B}_s^0 \rightarrow \rho^0 K^0$	$0.08^{+0.07}_{-0.04}$	0.10	—	—	$0.34^{+0.12}_{-0.09}$	0.61	—	—
$\bar{B}_s^0 \rightarrow \pi^0 K^{*0}$	$0.07^{+0.04}_{-0.02}$	0.08	—	—	$0.21^{+0.07}_{-0.04}$	0.25	—	—
$\bar{B}_s^0 \rightarrow \omega K^0$	$0.15^{+0.08}_{-0.05}$	0.14	—	—	$0.65^{+0.22}_{-0.17}$	0.51	—	—
$\bar{B}_s^0 \rightarrow K^0 \phi$	$0.16^{+0.10}_{-0.05}$	0.20	—	—	$0.24^{+0.05}_{-0.05}$	0.27	—	—
$\bar{B}_s^0 \rightarrow K^{*-} K^+$	$6.0^{+2.5}_{-1.9}$	9.03	—	—	$12.23^{+2.95}_{-3.41}$	$4.1^{+9.5}_{-3.2}$	19 ± 5	18.6 ± 4.70
$\bar{B}_s^0 \rightarrow K^- K^{*+}$	$4.7^{+2.7}_{-1.6}$		—	—	—	$5.5^{+15.1}_{-4.7}$		
$\bar{B}_s^0 \rightarrow \bar{K}^{*0} K^0$	$7.3^{+3.3}_{-2.1}$	9.95	—	—	$14.39^{+3.54}_{-2.93}$	$3.9^{+10.6}_{-3.5}$	20 ± 6	19.8 ± 5.7
$\bar{B}_s^0 \rightarrow \bar{K}^0 K^{*0}$	$4.3^{+2.3}_{-1.6}$		—	—	—	$4.2^{+14.0}_{-4.0}$		
$\bar{B}_s^0 \rightarrow \pi^- K^{*+}$	$7.6^{+3.0}_{-2.3}$	6.32	—	—	$3.96^{+1.41}_{-1.16}$	8.7	2.9 ± 1.1	3.0 ± 1.1
$\bar{B}_s^0 \rightarrow \rho^- K^+$	$17.8^{+7.89}_{-5.89}$	18.6	—	—	$15.9^{+6.5}_{-4.9}$	24.5	—	—

5 Conclusion

In this work, we revisit the decay processes $\bar{B}_s^0 \rightarrow PP$ and PV using the pQCD method, incorporating the contribution of ϕ_{B2} in the wave function and the effects of higher-order terms in the final-state meson DAs. Using the minimum χ^2 method, we determine the optimal value of ω_{B_s} and calculate the branching ratios and CP violation for these decay modes. Our results indicate that the inclusion of ϕ_{B2} has a noticeable impact on both the branching ratios and CP violation, providing a significant contribution to aligning the branching ratios of certain decay modes with experimental data. Thus, ϕ_{B2} should not be overlooked in the study of B_s meson weak decays.

Furthermore, while the contribution from higher-order terms in the final-state meson DAs is not as pronounced as that from ϕ_{B2} , it still plays a role in improving the accuracy of the theoretical predictions. From an experimental perspective, future measurements will likely become increasingly precise. Theoretically, both corrections from ϕ_{B2} and other potential interaction mechanisms are crucial, underscoring the need for continued efforts on both the experimental and theoretical fronts.

Acknowledgments

The work is supported by the National Natural Science Foundation of China (Grant Nos. 12275068, 12275067, 11705047), National Key R&D Program of China (Grant No. 2023YFA1606000), Science and Technology R&D Program Joint Fund Project of Henan Province (Grant No. 225200810030), Science and Technology Innovation Leading Talent Support Program of Henan Province, and Natural Science Foundation of Henan Province (Grant Nos. 222300420479, 242300420250).

A The amplitudes for $\bar{B}_s^0 \rightarrow PP$ and $\bar{B}_s^0 \rightarrow PV$

A.1 Amplitude building blocks

For conciseness, we adopt a compact notation for the hadronic WF components. In the framework of pQCD factorization, each hadron wave function is associated with a corresponding Sudakov factor, which takes the following specific form:

$$\begin{aligned}
\phi_P^a &= \phi_P^a(x_2)e^{-S_P}, & \phi_{P'}^a &= \phi_{P'}^a(x_3)e^{-S_{P'}}, \\
\phi_P^{p,t} &= r_P \phi_P^{p,t}(x_2)e^{-S_P}, & \phi_{P'}^{p,t} &= r_{P'} \phi_{P'}^{p,t}(x_3)e^{-S_{P'}}, \\
\phi_V^v &= f_V^\parallel \phi_V^v(x_3)e^{-S_V}, & \phi_V^{t,s} &= r_V f_V^\perp \phi_V^{t,s}(x_3)e^{-S_V}, \\
\phi_{B_1, B_2} &= \phi_{B_1, B_2}(x_1, b_1)e^{-S_{B_s}}, & \mathcal{C} &= \frac{\pi C_F}{N_c^2} m_{B_s}^4 f_{B_s} f_P.
\end{aligned} \tag{35}$$

where $r_P = \mu_P/m_{B_s}$, $r_V = m_V/m_{B_s}$.

The explicit expressions for the decay amplitudes \mathcal{A}_a^{LL} , \mathcal{A}_a^{LR} , and \mathcal{A}_a^{SP} corresponding to the factorizable emission diagram (a) in Fig. 5 are formulated as an illustrative case:

$$\begin{aligned}
\mathcal{A}_a^{LL} &= \int dx_1 dx_2 b_1 db_1 b_2 db_2 C_i(t_a) \alpha_s(t_a) S_t(x_2) H_{ab}(\alpha_g, \beta_a, b_1, b_2), \\
&\{\phi_{B_1}[\phi_M^a(1+x_2) + (\phi_M^p + \phi_M^t(\bar{x}_2 - x_2))] - \phi_{B_2}[\phi_M^a - (\phi_M^p + \phi_M^t)x_2]\}
\end{aligned} \tag{36}$$

$$\mathcal{A}_a^{LR} = -\mathcal{A}_a^{LL}, \tag{37}$$

$$\begin{aligned}
\mathcal{A}_a^{SP} &= 2r_{M'} \int dx_1 dx_2 b_1 db_1 b_2 db_2 C_i(t_a) \alpha_s(t_a) S_t(x_2) H_{ab}(\alpha_g, \beta_a, b_1, b_2) \\
&\{\phi_{B_1}[\phi_M^a + (\phi_M^p(2+x_2) - \phi_M^t x_2)] - \phi_{B_2}[\phi_M^a - (\phi_M^p + \phi_M^t)x_2]\}.
\end{aligned} \tag{38}$$

For a complete derivation of the framework underlying all diagrammatic components, we direct readers to the comprehensive treatments in [36, 37].

A.2 Decay amplitudes for $\bar{B}_s^0 \rightarrow PP$ processes

$$\begin{aligned}
& \mathcal{A}(\bar{B}_s^0 \rightarrow \pi^- K^+) \\
&= \frac{G_F}{\sqrt{2}} V_{ub} V_{ud}^* [a_1 \mathcal{A}_{ab}^{LL}(\pi^- K^+) + c_1 A_{cd}^{LL}(\pi^- K^+)] \\
&\quad - \frac{G_F}{\sqrt{2}} V_{tb} V_{td}^* [(a_4 + a_{10}) \mathcal{A}_{ab}^{LL}(\pi^- K^+) + (a_6 + a_8) A_{ab}^{SP}(\pi^- K^+) \\
&\quad + (c_3 + c_9) A_{cd}^{LL}(\pi^- K^+) \\
&\quad + (a_4 - \frac{a_{10}}{2}) A_{ef}^{LL}(\pi^- K^+) + (a_6 - \frac{a_8}{2}) A_{ef}^{SP}(\pi^- K^+) \\
&\quad + (c_3 - \frac{c_9}{2}) A_{gh}^{LL}(\pi^- K^+) + (c_5 - \frac{c_7}{2}) A_{gh}^{LR}(\pi^- K^+)], \tag{39}
\end{aligned}$$

$$\begin{aligned}
& \mathcal{A}(\bar{B}_s^0 \rightarrow \pi^+ \pi^-) = \sqrt{2} \mathcal{A}(\bar{B}_s^0 \rightarrow \pi^0 \pi^0) \\
&= \frac{G_F}{\sqrt{2}} V_{ub} V_{us}^* \{c_2 A_{gh}^{LL}\} - \frac{G_F}{\sqrt{2}} V_{tb} V_{ts}^* (2c_4 + 2c_6 + \frac{c_8}{2} + \frac{c_{10}}{2}) A_{gh}^{LL}(\pi^+ \pi^-), \tag{40}
\end{aligned}$$

$$\begin{aligned}
& \mathcal{A}(\bar{B}_s^0 \rightarrow \pi^0 K^0) \\
&= \frac{G_F}{2} V_{ub} V_{ud}^* \{a_2 \mathcal{A}_{ab}^{LL}(\pi^0, K^0) + c_2 \mathcal{A}_{cd}^{LL}(\pi^0, K^0)\} \\
&\quad - \frac{G_F}{2} V_{tb} V_{td}^* \{(-a_4 - \frac{3a_7}{2} + \frac{3a_9}{2} + \frac{a_{10}}{2}) \mathcal{A}_{ab}^{LL}(\pi^0, K^0) \\
&\quad + (-c_3 + \frac{3c_8}{2} + \frac{c_9}{2} + \frac{3c_{10}}{2}) \mathcal{A}_{cd}^{LL}(\pi^0, K^0) + (-a_6 + \frac{a_8}{2}) \mathcal{A}_{ab}^{SP}(\pi^0, K^0) \\
&\quad + (-a_6 + \frac{a_8}{2}) \mathcal{A}_{cd}^{SP}(\pi^0, K^0) + (-a_4 + \frac{a_{10}}{2}) \mathcal{A}_{ef}^{LL}(\pi^0, K^0) \\
&\quad + (-c_3 + \frac{c_9}{2}) \mathcal{A}_{gh}^{LL}(\pi^0, K^0) + (-c_5 + \frac{c_7}{2}) \mathcal{A}_{gh}^{LR}(\pi^0, K^0)\}, \tag{41}
\end{aligned}$$

$$\begin{aligned}
& \mathcal{A}(\bar{B}_s^0 \rightarrow K^- K^+) \\
&= \frac{G_F}{\sqrt{2}} \{V_{ub} V_{us}^* \{a_1 \mathcal{A}_{ab}^{LL}(K^-, K^+) + c_1 \mathcal{A}_{cd}^{LL}(K^-, K^+) + c_2 \mathcal{A}_{gh}^{LL}(K^-, K^+)\} \\
&\quad - \frac{G_F}{\sqrt{2}} V_{tb} V_{ts}^* \{(a_4 + a_{10}) \mathcal{A}_{ab}^{LL}(K^-, K^+) + (a_6 + a_8) \mathcal{A}_{ab}^{SP}(K^-, K^+)\}
\end{aligned}$$

$$\begin{aligned}
& + (c_3 + c_9)\mathcal{A}_{cd}^{LL}(K^-, K^+) + (c_5 + c_7)\mathcal{A}_{cd}^{LR}(K^-, K^+) \\
& + (a_6 - \frac{a_8}{2})\mathcal{A}_{ef}^{SP}(K^-, K^+) + (c_6 - \frac{c_8}{2})\mathcal{A}_{gh}^{SP}(K^-, K^+) \\
& + (c_3 + c_4 - \frac{c_9}{2} - \frac{c_{10}}{2})\mathcal{A}_{gh}^{LL}(K^-, K^+) + (c_5 - \frac{c_7}{2})\mathcal{A}_{gh}^{LR}(K^-, K^+) \\
& + (c_4 + \frac{C_{10}}{2})\mathcal{A}_{gh}^{LL}(K^+, K^-) + (c_6 + c_8)\mathcal{A}_{gh}^{SP}(K^+, K^-)\},
\end{aligned} \tag{42}$$

$$\begin{aligned}
& \mathcal{A}(\bar{B}_s^0 \rightarrow \bar{K}^0 K^0) \\
& = -\frac{G_F}{\sqrt{2}}V_{tb}V_{ts}^*\{(a_4 - \frac{1}{2}a_{10})A_{ab}^{LL}(\bar{K}^0 K^0) + (a_6 - \frac{1}{2}a_8)A_{ab}^{SP}(\bar{K}^0 K^0) \\
& \quad + (C_3 - \frac{1}{2}C_9)A_{cd}^{LL}(\bar{K}^0 K^0) + (C_5 - \frac{1}{2}C_7)A_{cd}^{LR}(\bar{K}^0 K^0) \\
& \quad + (a_6 - \frac{1}{2}a_8)A_{ef}^{SP}(\bar{K}^0 K^0) + (C_3 - \frac{1}{2}C_9 + C_4 - \frac{1}{2}C_{10})A_{gh}^{LL}(\bar{K}^0 K^0) \\
& \quad + (C_6 - \frac{1}{2}C_8)A_{gh}^{SP}(\bar{K}^0, K^0) + (C_5 - \frac{1}{2}C_7)A_{gh}^{LR}(\bar{K}^0 K^0) \\
& \quad + (C_4 - \frac{1}{2}C_{10})A_{gh}^{LL}(K^0, \bar{K}^0) + (C_6 - \frac{1}{2}C_8)A_{gh}^{SP}(K^0, \bar{K}^0)\}.
\end{aligned} \tag{43}$$

A.3 Decay amplitudes for $\bar{B}_s^0 \rightarrow PV$ processes

$$\begin{aligned}
& \mathcal{A}(\bar{B}_s^0 \rightarrow \rho^0 K^0) \\
& = \frac{G_F}{2}V_{ub}V_{ud}^*\{a_2A_{ab}^{LL}(\rho^0, K^0) + c_2A_{cd}^{LL}(\rho^0, K^0)\} \\
& \quad - \frac{G_F}{2}V_{tb}V_{td}^*\{(-a_4 + \frac{3a_7}{2} + \frac{3a_9}{2} + \frac{a_{10}}{2})A_{ab}^{LL}(\rho^0, K^0) \\
& \quad + (-c_3 + \frac{c_9}{2} + \frac{3c_{10}}{2})A_{cd}^{LL}(\rho^0, K^0) + (\frac{3c_8}{2})A_{cd}^{SP}(\rho^0, K^0) \\
& \quad + (-c_5 + \frac{c_7}{2})A_{cd}^{LR}(\rho^0, K^0) \\
& \quad + (-a_4 + \frac{a_{10}}{2})A_{ef}^{LL}(\rho^0, K^0) + (-a_6 + \frac{a_8}{2})A_{ef}^{SP}(\rho^0, K^0) \\
& \quad + (-c_3 + \frac{c_9}{2})A_{gh}^{LL}(\rho^0, K^0) + (-c_5 + \frac{c_7}{2})A_{gh}^{LR}(\rho^0, K^0)\},
\end{aligned} \tag{44}$$

$$\begin{aligned}
& \mathcal{A}(\bar{B}_s^0 \rightarrow \pi^0 K^{*0}) \\
&= \frac{G_F}{2} V_{ub} V_{ud}^* \{a_2 A_{ab}^{LL}(\pi^0, K^{*0}) + c_2 A_{cd}^{LL}(\pi^0, K^{*0})\} \\
&\quad - \frac{G_F}{2} V_{tb} V_{td}^* \{(-a_4 - \frac{3a_7}{2} + \frac{a_{10}}{2} + \frac{3a_9}{2}) A_{ab}^{LL}(\pi^0, K^{*0}) \\
&\quad - (-a_6 + \frac{a_8}{2}) A_{ab}^{SP}(\pi^0, K^{*0}) + (-c_3 + \frac{3c_8}{2} + \frac{c_9}{2} + \frac{3c_{10}}{2}) A_{cd}^{LL}(\pi^0, K^{*0}) \\
&\quad + (-a_4 + \frac{a_{10}}{2}) A_{ef}^{LL}(\pi^0, K^{*0}) + (-a_6 + \frac{a_8}{2}) A_{ef}^{SP}(\pi^0, K^{*0}) \\
&\quad + (-c_3 + \frac{c_9}{2}) A_{gh}^{LL}(\pi^0, K^{*0}) - (-c_5 + \frac{c_7}{2}) A_{gh}^{LR}(\pi^0, K^{*0})\}, \tag{45}
\end{aligned}$$

$$\begin{aligned}
& \mathcal{A}(\bar{B}_s^0 \rightarrow \omega K^0) \\
&= \frac{G_F}{2} V_{ub} V_{ud}^* \{a_2 A_{ab}^{LL}(\omega, K^0) + c_2 A_{cd}^{LL}(\omega, K^0)\} \\
&\quad + \frac{G_F}{2} V_{tb} V_{td}^* \{(2a_3 + a_4 + 2a_5 + \frac{a_7}{2} + \frac{a_9}{2} - \frac{a_{10}}{2}) A_{ab}^{LL}(\omega, K^0) \\
&\quad + (c_3 + 2c_4 - \frac{c_9}{2} + \frac{c_{10}}{2}) A_{cd}^{LL}(\omega, K^0) - (2c_6 + \frac{c_8}{2}) A_{cd}^{SP}(\omega, K^0) \\
&\quad + (c_5 - \frac{c_7}{2}) A_{cd}^{LR}(\omega, K^0) \\
&\quad + (a_4 - \frac{a_{10}}{2}) A_{ef}^{LL}(\omega, K^0) + (a_6 - \frac{a_8}{2}) A_{ef}^{SP}(\omega, K^0) \\
&\quad + (c_3 - \frac{c_9}{2}) A_{gh}^{LL}(\omega, K^0) + (c_5 - \frac{c_7}{2}) A_{gh}^{LR}(\omega, K^0)\}, \tag{46}
\end{aligned}$$

$$\begin{aligned}
& \mathcal{A}(\bar{B}_s^0 \rightarrow K^0 \phi) \\
&= -\frac{G_F}{\sqrt{2}} V_{tb} V_{td}^* \{(a_3 + a_5 - \frac{a_7}{2} - \frac{a_9}{2}) A_{ab}^{LL}(\phi, K^0) + (a_4 - \frac{a_{10}}{2}) A_{ab}^{LL}(K^0, \phi) \\
&\quad + (a_6 - \frac{a_8}{2}) A_{ab}^{SP}(K^0, \phi) \\
&\quad + (c_4 - \frac{C_{10}}{2}) A_{cd}^{LL}(\phi, K^0) + (c_3 - \frac{C_9}{2}) A_{cd}^{LL}(K^0, \phi) \\
&\quad - (c_6 - \frac{c_8}{2}) A_{cd}^{SP}(\phi, K^0) - (c_5 - \frac{c_7}{2}) A_{cd}^{LR}(K^0, \phi)\}
\end{aligned}$$

$$\begin{aligned}
& + (a_4 - \frac{a_{10}}{2})A_{ef}^{LL}(K^0, \phi) - (a_6 - \frac{a_8}{2})A_{ef}^{SP}(K^0, \phi) \\
& + (c_3 - \frac{C_9}{2})A_{gh}^{LL}(K^0, \phi) - (c_5 - \frac{c_7}{2})A_{gh}^{LR}(K^0, \phi)\},
\end{aligned} \tag{47}$$

$$\begin{aligned}
& \mathcal{A}(\bar{B}_s^0 \rightarrow K^{*-} K^+) \\
& = \frac{G_F}{\sqrt{2}} \{V_{ub}V_{us}^* \{a_1 A_{ab}^{LL}(K^{*-}, K^+) + c_1 A_{cd}^{LL}(K^{*-}, K^+) + a_2 A_{ef}^{LL}(K^+, K^{*-}) + c_2 A_{gh}^{LL}(K^+, K^{*-})\} \\
& - \frac{G_F}{\sqrt{2}} V_{tb}V_{ts}^* \{(a_4 + a_{10})A_{ab}^{LL}(K^{*-}, K^+) + (c_3 + c_9)A_{cd}^{LL}(K^{*-}, K^+) + (c_5 + c_7)A_{cd}^{LR}(K^{*-}, K^+) \\
& + (a_3 + a_4 - a_5 + \frac{a_7}{2} - \frac{a_9}{2} - \frac{a_{10}}{2})A_{ef}^{LL}(K^{*-}, K^+) \\
& + (a_6 - \frac{a_8}{2})A_{ef}^{SP}(K^{*-}, K^+) + (a_3 - a_5 - a_7 + a_9)A_{ef}^{LL}(K^+, K^{*-}) \\
& + (c_5 - \frac{c_7}{2})A_{gh}^{LR}(K^{*-}, K^+) + (c_3 + c_4 - \frac{c_9}{2} - \frac{c_{10}}{2})A_{gh}^{LL}(K^{*-}, K^+) \\
& - (c_6 - \frac{c_8}{2})A_{gh}^{SP}(K^{*-}, K^+) + (c_4 + c_{10})A_{gh}^{LL}(K^+, K^{*-}) \\
& - (c_6 + c_8)A_{gh}^{SP}(K^+, K^{*-})\},
\end{aligned} \tag{48}$$

$$\begin{aligned}
& \mathcal{A}(\bar{B}_s^0 \rightarrow K^- K^{*+}) \\
& = \frac{G_F}{\sqrt{2}} \{V_{ub}V_{us}^* \{a_1 A_{ab}^{LL}(K^-, K^{*+}) + c_1 A_{cd}^{LL}(K^-, K^{*+}) + a_2 A_{ef}^{LL}(K^{*+}, K^-) + c_2 A_{gh}^{LL}(K^{*+}, K^-)\} \\
& - \frac{G_F}{\sqrt{2}} V_{tb}V_{ts}^* \{(a_4 + a_{10})A_{ab}^{LL}(K^-, K^{*+}) - (a_6 + a_8)A_{ab}^{SP}(K^-, K^{*+}) - (c_6 + c_8)A_{gh}^{SP}(K^{*+}, K^-) \\
& + (c_3 + c_9)A_{cd}^{LL}(K^-, K^{*+}) - (c_5 + c_7)A_{cd}^{LL}(K^-, K^{*+}) \\
& + (a_3 + a_4 - a_5 + \frac{a_7}{2} - \frac{a_9}{2} - \frac{a_{10}}{2})A_{ef}^{LL}(K^-, K^{*+}) \\
& + (a_3 - a_5 - a_7 + a_9)A_{ef}^{LL}(K^{*+}, K^-) - (a_6 - \frac{a_8}{2})A_{ef}^{SP}(K^-, K^{*+}) \\
& - (c_5 - \frac{c_7}{2})A_{gh}^{LR}(K^-, K^{*+}) + (c_3 + c_4 - \frac{C_9}{2} - \frac{C_{10}}{2})A_{gh}^{LL}(K^-, K^{*+}) \\
& - (c_6 - \frac{c_8}{2})A_{gh}^{SP}(K^-, K^{*+}) + (c_4 + c_{10})A_{gh}^{LL}(K^{*+}, K^-)\},
\end{aligned} \tag{49}$$

$$\begin{aligned}
& \mathcal{A}(\bar{B}_s^0 \rightarrow \bar{K}^{*0} K^0) \\
&= -\frac{G_F}{\sqrt{2}} V_{tb} V_{ts}^* \{ (a_4 - \frac{a_{10}}{2}) A_{ab}^{LL}(\bar{K}^{*0}, K^0) + (c_3 - \frac{c_9}{2}) A_{cd}^{LL}(\bar{K}^{*0}, K^0) \\
&\quad + (c_5 - \frac{c_7}{2}) A_{cd}^{LR}(\bar{K}^{*0}, K^0) + (a_6 - \frac{a_8}{2}) A_{ef}^{SP}(\bar{K}^{*0}, K^0) \\
&\quad + (a_3 + a_4 - a_5 + \frac{a_7}{2} - \frac{a_9}{2} - \frac{a_{10}}{2}) A_{ef}^{LL}(\bar{K}^{*0}, K^0) \\
&\quad + (c_3 + c_4 - \frac{c_9}{2} - \frac{c_{10}}{2}) A_{gh}^{LL}(\bar{K}^{*0}, K^0) + (c_4 - \frac{c_{10}}{2}) A_{gh}^{LL}(K^0, \bar{K}^{*0}) \\
&\quad + (c_5 - \frac{c_7}{2}) A_{gh}^{LR}(\bar{K}^{*0}, K^0) - (c_6 - \frac{c_8}{2}) A_{gh}^{SP}(K^0, \bar{K}^{*0}) \\
&\quad + (a_3 - a_5 + \frac{a_7}{2} - \frac{a_9}{2}) A_{ef}^{LL}(K^0, \bar{K}^{*0}) - (c_6 - \frac{c_8}{2}) A_{gh}^{SP}(\bar{K}^{*0}, K^0) \}, \tag{50}
\end{aligned}$$

$$\begin{aligned}
& \mathcal{A}(\bar{B}_s^0 \rightarrow \bar{K}^0 K^{*0}) \\
&= -\frac{G_F}{\sqrt{2}} V_{tb} V_{ts}^* \{ (a_4 - \frac{a_{10}}{2}) A_{ab}^{LL}(\bar{K}^0, K^{*0}) + (a_6 - \frac{a_8}{2}) A_{ab}^{SP}(\bar{K}^0, K^{*0}) \\
&\quad + (c_3 - \frac{c_9}{2}) A_{cd}^{LL}(\bar{K}^0, K^{*0}) - (c_5 - \frac{c_7}{2}) A_{cd}^{LR}(\bar{K}^0, K^{*0}) \\
&\quad + (a_3 + a_4 - a_5 + \frac{a_7}{2} - \frac{a_9}{2} - \frac{a_{10}}{2}) A_{ef}^{LL}(\bar{K}^0, K^{*0}) \\
&\quad - (a_6 - \frac{a_8}{2}) A_{ef}^{SP}(\bar{K}^0, K^{*0}) \\
&\quad + (c_3 + c_4 - \frac{c_9}{2} - \frac{c_{10}}{2}) A_{gh}^{LL}(\bar{K}^0, K^{*0}) + (c_4 - \frac{c_{10}}{2}) A_{gh}^{LL}(K^{*0}, \bar{K}^0) \\
&\quad - (c_5 - \frac{c_7}{2}) A_{gh}^{LR}(\bar{K}^0, K^{*0}) - (c_6 - \frac{c_8}{2}) A_{gh}^{SP}(K^{*0}, \bar{K}^0) \\
&\quad + (a_3 - a_5 + \frac{a_7}{2} - \frac{a_9}{2}) A_{ef}^{LL}(K^{*0}, \bar{K}^0) - (c_6 - \frac{c_8}{2}) A_{gh}^{SP}(\bar{K}^0, K^{*0}) \}, \tag{51}
\end{aligned}$$

$$\begin{aligned}
& \mathcal{A}(\bar{B}_s^0 \rightarrow \pi^- K^{*+}) \\
&= \frac{G_F}{\sqrt{2}} V_{ub} V_{ud}^* \{ a_1 A_{ab}^{LL}(\pi^-, K^{*+}) + c_1 A_{cd}^{LL}(\pi^-, K^{*+}) \} \\
&\quad - \frac{G_F}{\sqrt{2}} V_{tb} V_{td}^* \{ (a_4 + a_{10}) A_{ab}^{LL}(\pi^-, K^{*+}) - (a_6 + a_8) A_{ab}^{SP}(\pi^-, K^{*+}) + (c_3 + c_9) A_{cd}^{LL}(\pi^-, K^{*+}) \\
&\quad - (c_5 - \frac{c_7}{2}) A_{cd}^{LR}(\pi^-, K^{*+}) - (a_6 - \frac{a_8}{2}) A_{ef}^{SP}(\pi^-, K^{*+}) + (a_3 - a_5 + \frac{a_7}{2} - \frac{a_9}{2}) A_{ef}^{LL}(\pi^-, K^{*+}) \\
&\quad - (c_6 - \frac{c_8}{2}) A_{gh}^{SP}(\pi^-, K^{*+}) \},
\end{aligned}$$

$$\begin{aligned}
& + (a_4 - \frac{a_{10}}{2})A_{ef}^{LL}(\pi^-, K^{*+}) - (a_6 - \frac{a_8}{2})A_{ef}^{SP}(\pi^-, K^{*+}) \\
& + (c_3 - \frac{c_9}{2})A_{gh}^{LL}(\pi^-, K^{*+}) + (c_5 - \frac{c_7}{2})A_{gh}^{LR}(\pi^-, K^{*+})\},
\end{aligned} \tag{52}$$

$$\begin{aligned}
& \mathcal{A}(\bar{B}_s^0 \rightarrow \rho^- K^+) \\
& = \frac{G_F}{\sqrt{2}} V_{ub} V_{ud}^* \{a_1 A_{ab}^{LL}(\rho^-, K^+) + c_1 A_{cd}^{LL}(\rho^-, K^+)\} \\
& - \frac{G_F}{\sqrt{2}} V_{tb} V_{td}^* \{(a_4 + a_{10})A_{ab}^{LL}(\rho^-, K^+) + (c_3 + c_9)A_{cd}^{LL}(\rho^-, K^+) + (c_5 + c_7)A_{cd}^{LR}(\rho^-, K^+) \\
& + (a_4 - \frac{a_{10}}{2})A_{ef}^{LL}(\rho^-, K^+) + (a_6 - \frac{a_8}{2})A_{ef}^{SP}(\rho^-, K^+) \\
& + (c_3 - \frac{c_9}{2})A_{gh}^{LL}(\rho^-, K^+) + (c_5 - \frac{c_7}{2})A_{gh}^{LR}(\rho^-, K^+)\}.
\end{aligned} \tag{53}$$

References

- [1] W. Altmannshofer, et al. (Belle-II Collaboration), The Belle II Physics Book, PTEP 2019 (2019) 123C01. doi:10.1093/ptep/ptz106. arXiv:1808.10567, [Erratum: PTEP 2020, 029201 (2020)].
- [2] R. Aaij, et al. (LHCb Collaboration), Physics case for an LHCb Upgrade II - Opportunities in flavour physics, and beyond, in the HL-LHC era (2018). arXiv:1808.08865.
- [3] W. Abdallah, et al. (CEPC Study Group), CEPC Technical Design Report: Accelerator, Radiat. Detect. Technol. Methods 8 (2024) 1–1105. doi:10.1007/s41605-024-00463-y. arXiv:2312.14363, [Erratum: Radiat.Detect.Technol.Methods None, (2024)].
- [4] A. Abada, et al. (FCC), FCC Physics Opportunities: Future Circular Collider Conceptual Design Report Volume 1, Eur. Phys. J. C 79 (2019) 474. doi:10.1140/epjc/s10052-019-6904-3.
- [5] S. Navas, et al. (Particle Data Group), Review of particle physics, Phys. Rev. D 110 (2024) 030001. doi:10.1103/PhysRevD.110.030001.
- [6] J. Abdallah, et al. (DELPHI Collaboration), A Measurement of the branching fractions of the b quark into charged and neutral b hadrons, Phys. Lett. B 576 (2003) 29–42. doi:10.1016/j.physletb.2003.09.070. arXiv:hep-ex/0311005.

- [7] R. Aaij, et al. (LHCb Collaboration), Precise measurement of the f_s/f_d ratio of fragmentation fractions and of B_s^0 decay branching fractions, Phys. Rev. D 104 (2021) 032005. doi:10.1103/PhysRevD.104.032005. arXiv:2103.06810.
- [8] T. Aaltonen, et al. (CDF Collaboration), Evidence for the charmless annihilation decay mode $B_s^0 \rightarrow \pi^+\pi^-$, Phys. Rev. Lett. 108 (2012) 211803. doi:10.1103/PhysRevLett.108.211803. arXiv:1111.0485.
- [9] T. Aaltonen, et al. (CDF Collaboration), Observation of New Charmless Decays of Bottom Hadrons, Phys. Rev. Lett. 103 (2009) 031801. doi:10.1103/PhysRevLett.103.031801. arXiv:0812.4271.
- [10] T. Aaltonen, et al. (CDF Collaboration), Measurements of Direct CP Violating Asymmetries in Charmless Decays of Strange Bottom Mesons and Bottom Baryons, Phys. Rev. Lett. 106 (2011) 181802. doi:10.1103/PhysRevLett.106.181802. arXiv:1103.5762.
- [11] T. A. Aaltonen, et al. (CDF Collaboration), Measurements of Direct CP -Violating Asymmetries in Charmless Decays of Bottom Baryons, Phys. Rev. Lett. 113 (2014) 242001. doi:10.1103/PhysRevLett.113.242001. arXiv:1403.5586.
- [12] C. C. Peng, et al. (Belle Collaboration), Search for $B_s^0 \rightarrow hh$ Decays at the $\Upsilon(5S)$ Resonance, Phys. Rev. D 82 (2010) 072007. doi:10.1103/PhysRevD.82.072007. arXiv:1006.5115.
- [13] B. Pal, et al. (Belle Collaboration), Observation of the decay $B_s^0 \rightarrow K^0\bar{K}^0$, Phys. Rev. Lett. 116 (2016) 161801. doi:10.1103/PhysRevLett.116.161801. arXiv:1512.02145.
- [14] R. Aaij, et al. (LHCb Collaboration), Observation of the annihilation decay mode $B^0 \rightarrow K^+K^-$, Phys. Rev. Lett. 118 (2017) 081801. doi:10.1103/PhysRevLett.118.081801. arXiv:1610.08288.
- [15] R. Aaij, et al. (LHCb Collaboration), Measurement of b -hadron branching fractions for two-body decays into charmless charged hadrons, JHEP 10 (2012) 037. doi:10.1007/JHEP10(2012)037. arXiv:1206.2794.
- [16] R. Aaij, et al. (LHCb Collaboration), Measurement of the branching fraction of the decay $B_s^0 \rightarrow K_S^0 K_S^0$, Phys. Rev. D 102 (2020) 012011. doi:10.1103/PhysRevD.102.012011. arXiv:2002.08229.
- [17] R. Aaij, et al. (LHCb Collaboration), Amplitude analysis of $B_s^0 \rightarrow K_S^0 K^\pm \pi^\mp$ decays, JHEP 06 (2019) 114. doi:10.1007/JHEP06(2019)114. arXiv:1902.07955.

- [18] R. Aaij, et al. (LHCb Collaboration), Observation of $B_s^0 \rightarrow K^{*\pm} K^\mp$ and evidence for $B_s^0 \rightarrow K^{*-} \pi^+$ decays, *New J. Phys.* 16 (2014) 123001. doi:10.1088/1367-2630/16/12/123001. [arXiv:1407.7704](#).
- [19] R. Aaij, et al. (LHCb Collaboration), Measurement of CP asymmetries in two-body $B_{(s)}^0$ -meson decays to charged pions and kaons, *Phys. Rev. D* 98 (2018) 032004. doi:10.1103/PhysRevD.98.032004. [arXiv:1805.06759](#).
- [20] R. Aaij, et al. (LHCb Collaboration), Observation of CP violation in two-body $B_{(s)}^0$ -meson decays to charged pions and kaons, *JHEP* 03 (2021) 075. doi:10.1007/JHEP03(2021)075. [arXiv:2012.05319](#).
- [21] R. Aaij, et al. (LHCb Collaboration), First measurement of time-dependent CP violation in $B_s^0 \rightarrow K^+ K^-$ decays, *JHEP* 10 (2013) 183. doi:10.1007/JHEP10(2013)183. [arXiv:1308.1428](#).
- [22] S. Banerjee, et al. (Heavy Flavor Averaging Group (HFLAV)), Averages of b -hadron, c -hadron, and τ -lepton properties as of 2023 (2024). [arXiv:2411.18639](#).
- [23] M. Beneke, M. Neubert, QCD factorization for $B \rightarrow PP$ and $B \rightarrow PV$ decays, *Nucl. Phys. B* 675 (2003) 333–415. doi:10.1016/j.nuclphysb.2003.09.026. [arXiv:hep-ph/0308039](#).
- [24] J.-f. Sun, G.-h. Zhu, D.-s. Du, Phenomenological analysis of charmless decays $B_s \rightarrow PP, PV$, with QCD factorization, *Phys. Rev. D* 68 (2003) 054003. doi:10.1103/PhysRevD.68.054003. [arXiv:hep-ph/0211154](#).
- [25] H.-Y. Cheng, C.-K. Chua, QCD Factorization for Charmless Hadronic B_s Decays Revisited, *Phys. Rev. D* 80 (2009) 114026. doi:10.1103/PhysRevD.80.114026. [arXiv:0910.5237](#).
- [26] Q. Chang, J. Sun, Y. Yang, X. Li, A combined fit on the annihilation corrections in $B_{u,d,s} \rightarrow PP$ decays within QCDF, *Phys. Lett. B* 740 (2015) 56–60. doi:10.1016/j.physletb.2014.11.027. [arXiv:1409.2995](#).
- [27] A. R. Williamson, J. Zupan, Two body B decays with isosinglet final states in SCET, *Phys. Rev. D* 74 (2006) 014003. doi:10.1103/PhysRevD.74.014003. [arXiv:hep-ph/0601214](#), [Erratum: *Phys.Rev.D* 74, 03901 (2006)].
- [28] Y. Li, C.-D. Lu, Z.-J. Xiao, X.-Q. Yu, Branching ratio and CP asymmetry of $B_s \rightarrow \pi^+ \pi^-$ decays in the perturbative QCD approach, *Phys. Rev. D* 70 (2004) 034009. doi:10.1103/PhysRevD.70.034009. [arXiv:hep-ph/0404028](#).

- [29] A. Ali, G. Kramer, Y. Li, C.-D. Lu, Y.-L. Shen, W. Wang, Y.-M. Wang, Charmless non-leptonic B_s decays to PP , PV and VV final states in the pQCD approach, Phys. Rev. D 76 (2007) 074018. doi:10.1103/PhysRevD.76.074018. arXiv:hep-ph/0703162.
- [30] Z.-J. Xiao, W.-F. Wang, Y.-y. Fan, Revisiting the pure annihilation decays $B_s \rightarrow \pi^+\pi^-$ and $B^0 \rightarrow K^+K^-$: the data and the pQCD predictions, Phys. Rev. D 85 (2012) 094003. doi:10.1103/PhysRevD.85.094003. arXiv:1111.6264.
- [31] J.-J. Wang, D.-T. Lin, W. Sun, Z.-J. Ji, S. Cheng, Z.-J. Xiao, $\bar{B}_s^0 \rightarrow K\pi, KK$ decays and effects of the next-to-leading order contributions, Phys. Rev. D 89 (2014) 074046. doi:10.1103/PhysRevD.89.074046. arXiv:1402.6912.
- [32] D.-C. Yan, X. Liu, Z.-J. Xiao, Anatomy of $B_s \rightarrow PP$ decays and effects of the next-to-leading order contributions in the perturbative QCD approach, Nucl. Phys. B 946 (2019) 114705. doi:10.1016/j.nuclphysb.2019.114705. arXiv:1906.01442.
- [33] D.-C. Yan, P. Yang, X. Liu, Z.-J. Xiao, Anatomy of $B_s \rightarrow PV$ decays and effects of next-to-leading order contributions in the perturbative QCD factorization approach, Nucl. Phys. B 931 (2018) 79–104. doi:10.1016/j.nuclphysb.2018.04.007. arXiv:1707.06043.
- [34] H.-Y. Cheng, S. Oh, Flavor SU(3) symmetry and QCD factorization in $B \rightarrow PP$ and PV decays, JHEP 09 (2011) 024. doi:10.1007/JHEP09(2011)024. arXiv:1104.4144.
- [35] H.-Y. Cheng, C.-W. Chiang, A.-L. Kuo, Updating $B \rightarrow PP, VP$ decays in the framework of flavor symmetry, Phys. Rev. D 91 (2015) 014011. doi:10.1103/PhysRevD.91.014011. arXiv:1409.5026.
- [36] Y. Yang, L. Lang, X. Zhao, J. Huang, J. Sun, Reinvestigating the $B \rightarrow PP$ decays by including the contributions from ϕ_{B2} , Phys. Rev. D 103 (2021) 056006. doi:10.1103/PhysRevD.103.056006. arXiv:2012.10581.
- [37] Y. Yang, X. Zhao, L. Lang, J. Huang, J. Sun, Reinvestigating $B \rightarrow PV$ decays by including contributions from ϕ_{B2} with the perturbative QCD approach *, Chin. Phys. C 46 (2022) 083103. doi:10.1088/1674-1137/ac6573. arXiv:2201.12834.
- [38] P. Ball, V. M. Braun, A. Lenz, Higher-twist distribution amplitudes of the K meson in QCD, JHEP 05 (2006) 004. doi:10.1088/1126-6708/2006/05/004. arXiv:hep-ph/0603063.
- [39] T. Huang, X.-G. Wu, Consistent calculation of the $B \rightarrow \pi$ transition form-factor in the whole physical region, Phys. Rev. D 71 (2005) 034018. doi:10.1103/PhysRevD.71.034018. arXiv:hep-ph/0412417.

- [40] T. Kurimoto, Uncertainty in the leading order PQCD calculations of B meson decays, Phys. Rev. D 74 (2006) 014027. doi:10.1103/PhysRevD.74.014027. arXiv:hep-ph/0605112.
- [41] S. Cheng, Y.-Y. Fan, X. Yu, C.-D. Lü, Z.-J. Xiao, The NLO twist-3 contributions to $B \rightarrow \pi$ form factors in k_T factorization, Phys. Rev. D 89 (2014) 094004. doi:10.1103/PhysRevD.89.094004. arXiv:1402.5501.
- [42] C.-D. Lu, M.-Z. Yang, $B \rightarrow \pi\rho, \pi\omega$ decays in perturbative QCD approach, Eur. Phys. J. C 23 (2002) 275–287. doi:10.1007/s100520100878. arXiv:hep-ph/0011238.
- [43] S. Descotes-Genon, C. T. Sachrajda, Sudakov effects in $B \rightarrow \pi\ell\nu_\ell$ form-factors, Nucl. Phys. B 625 (2002) 239–278. doi:10.1016/S0550-3213(02)00017-2. arXiv:hep-ph/0109260.
- [44] Z.-T. Wei, M.-Z. Yang, The Systematic study of $B \rightarrow \pi$ form-factors in pQCD approach and its reliability, Nucl. Phys. B 642 (2002) 263–289. doi:10.1016/S0550-3213(02)00623-5. arXiv:hep-ph/0202018.
- [45] Y. Y. Keum, H.-N. Li, A. I. Sanda, Penguin enhancement and $B \rightarrow K\pi$ decays in perturbative QCD, Phys. Rev. D 63 (2001) 054008. doi:10.1103/PhysRevD.63.054008. arXiv:hep-ph/0004173.
- [46] P. Ball, Theoretical update of pseudoscalar meson distribution amplitudes of higher twist: The Nonsinglet case, JHEP 01 (1999) 010. doi:10.1088/1126-6708/1999/01/010. arXiv:hep-ph/9812375.
- [47] P. Ball, G. W. Jones, Twist-3 distribution amplitudes of K^* and ϕ mesons, JHEP 03 (2007) 069. doi:10.1088/1126-6708/2007/03/069. arXiv:hep-ph/0702100.
- [48] T. Kurimoto, H.-n. Li, A. I. Sanda, Leading power contributions to $B \rightarrow \pi, \rho$ transition form-factors, Phys. Rev. D 65 (2002) 014007. doi:10.1103/PhysRevD.65.014007. arXiv:hep-ph/0105003.
- [49] J. Hua, H.-n. Li, C.-D. Lu, W. Wang, Z.-P. Xing, Global analysis of hadronic two-body B decays in the perturbative QCD approach, Phys. Rev. D 104 (2021) 016025. doi:10.1103/PhysRevD.104.016025. arXiv:2012.15074.
- [50] J. Liu, R. Zhou, Z.-J. Xiao, $B_s \rightarrow PP$ decays and the NLO contributions in the pQCD Approach (2008). arXiv:0812.2312.